






## Article

# The Effect of Sodium and Magnesium Sulfate on Physico-Mechanical and Microstructural Properties of Kaolin and Ceramic Powder-Based Geopolymer Mortar

Mehmet Kaya <sup>1</sup>, Fuat Köksal <sup>1</sup>, Mehrab Nodehi <sup>2</sup>, Muhammed Bayram <sup>2</sup>, Osman Gencil <sup>3,\*</sup> and Togay Ozbakkaloglu <sup>2,\*</sup>

<sup>1</sup> Department of Civil Engineering, Yozgat Bozok University, Yozgat 66900, Turkey

<sup>2</sup> Ingram School of Engineering, Texas State University, San Marcos, TX 78666, USA

<sup>3</sup> Civil Engineering Department, Faculty of Engineering, Architecture and Design, Bartin University, Bartin 74100, Turkey

\* Correspondence: ogencil@bartin.edu.tr (O.G.); togay.oz@txstate.edu (T.O.)

**Abstract:** Recent trends in reducing the ecological footprint of the construction industry have increased the attention surrounding the use of alternative binding systems. Among the most promising are geopolymer binders, which were found to have the capability to substantially reduce the environmental impact of Portland cement use. However, even the use of this alternative binding system is known to be heavily dependent on the use of industrial byproducts, such as precursors and an alkaline source, produced through an energy intensive process. To address this and provide a greener route for this binding system, this study adopts the use of natural kaolin and raw ceramic powder as the main precursors. The activation process is performed by using solid potassium hydroxide in conjunction with sodium and magnesium sulfate, which are naturally available, to produce geopolymers. To assess the resulting geopolymer samples, 28 mixes are produced and a series of physico-mechanical and microstructural analyses is conducted. The results show that the use of ceramic powder can improve the physico-mechanical properties by reducing porosity. This, however, requires a relatively higher alkalinity for activation and strength development. These findings are further confirmed with the XRD and FTIR results. Nonetheless, the use of ceramic powder with sodium and magnesium sulfate is found to result in a more coherent and homogenous microstructure, compared to the geopolymers produced with potassium hydroxide and kaolin. The findings of this study point to the suitability of using sodium and magnesium sulfate for the cleaner production of kaolin and ceramic powder-based geopolymers.

**Keywords:** cleaner production of geopolymer; ceramic powder; kaolin; geopolymer; sodium sulfate; magnesium sulfate



**Citation:** Kaya, M.; Köksal, F.; Nodehi, M.; Bayram, M.; Gencil, O.; Ozbakkaloglu, T. The Effect of Sodium and Magnesium Sulfate on Physico-Mechanical and Microstructural Properties of Kaolin and Ceramic Powder-Based Geopolymer Mortar. *Sustainability* **2022**, *14*, 13496. <https://doi.org/10.3390/su142013496>

Academic Editors: Marijana Hadzima-Nyarko and Dorin Radu

Received: 22 September 2022

Accepted: 2 October 2022

Published: 19 October 2022

**Publisher's Note:** MDPI stays neutral with regard to jurisdictional claims in published maps and institutional affiliations.



**Copyright:** © 2022 by the authors. Licensee MDPI, Basel, Switzerland. This article is an open access article distributed under the terms and conditions of the Creative Commons Attribution (CC BY) license (<https://creativecommons.org/licenses/by/4.0/>).

## 1. Introduction

The increasing socioeconomic effect of climate change and natural disasters has caused a growing body of international and intergovernmental entities to advocate carbon neutrality and aim for a net-zero carbon dioxide production. Yet, the incorporation of carbon neutrality into construction requires a fundamental shift from the commonly accepted use of polluting practices, such as the heavy dependence on ordinary Portland cement (OPC) to alternative cementing materials and systems, such as geopolymer technology [1]. According to previous studies that conducted a life cycle assessment (cradle-to-grave), for instance, geopolymer binders have been reported to be able to reduce the overall CO<sub>2</sub> production of concrete by approximately 40% [2,3] to 75% [4] when compared to Portland cement concrete. Although this reduction rate was considerable [5–7], after approximately a century of development, geopolymer binders are not commonly being used for major infrastructural projects. In part, this could be due to the need for the utilization of polluting

and often hazardous liquid activators, such as sodium silicate, which is produced through the melting of silicon dioxide and sodium carbonate at a high temperature of approximately 1200–1400 °C [8]. As a result, previous studies reported that the activators' production process is the main polluting ingredient of geopolymer binders [9], accounting for 40% [10] to 60% [11] of the total ecological footprint of this binder system. In that respect, to avoid the use of hazardous and polluting liquid activators, naturally available and artificially produced solid activators with a lower ecological footprint have recently been introduced [12]. According to Passuello et al. [4], alternative activators, to those artificially produced, can reduce the environmental impact of geopolymer production by up to 60%. Nonetheless, one of the main technical challenges facing the transition to the cleaner and higher use of this binding system is the use of naturally occurring precursors and activators. In terms of precursors, industrial byproducts, such as coal fly ash and blast furnace slag, have been used for a long time, and become the key components of geopolymer technology [7,13,14]. Yet, recent advances in the utilization of advanced technologies in energy production (e.g., coal-free electricity generation), as well as carbon-free steel technologies (through the use of green hydrogen), all refer to the potential future shortcomings of such commonly utilized precursors.

To address this, recent studies have incorporated the use of alternative cementitious materials, such as naturally available precursors for geopolymer concrete production [15]. In general, naturally occurring aluminosilicate materials for use in geopolymer binders include a broad range of natural pozzolans [16–21] and clay minerals [22–24]. These materials are known to have a high content of reactive silica and alumina that can be used in geopolymer synthesis with a low ecological footprint [16]. Natural kaolin, for instance, is a layered silicate mineral that is produced naturally through the chemical weathering of minerals, such as feldspar, that are rich in alumina and silicate [25,26]. In general, kaolin is often referred to as China clay, and its main components are kaolinite and quartz, in addition to other minerals, such as feldspar, illite and montmorillonite [27]. The term kaolin generally refers to a both raw and uncalcined material, as well as a refined commercial product that is produced when kaolin is thermally treated at temperatures of 500–800 °C, which can chemically react with  $\text{Ca}(\text{OH})_2$  [28].

Kaolin has major uses in ceramics, as well as paint, rubber and plastics production, mainly as a filler material [26]. In addition, uncalcined kaolin has been successfully used as a filler [29] and precursor [28] in previous studies. With approximately 45 million tons of kaolin produced annually [30], it can be a suitable precursor for geopolymer binders, which require less energy for their production and are more environmentally friendly [31,32].

As discussed for kaolin, ceramic powder waste material is mostly produced in the polishing of ceramic tiles [33–35] and has a chemical composition rich in silica and alumina [36,37]. Most commonly, ceramic waste is landfilled and considered a solid waste material. Nonetheless, recent studies (e.g., [38–40]) successfully used this material as a supplement precursor or filler in concrete [41]. In that respect, with a production of approximately 12.6 million square meters annually [42], ceramic powder can be a suitable waste material for further use in geopolymeric binders.

According to the literature, although the use of natural pozzolans, such as kaolin, has been found to have certain suitability, most often, a low reactivity rate and geopolymerization are reported, which require the use of a higher activator content [43]. To address this, previous studies adopted novel methods, such as increasing the surface area of pozzolanic materials [44], the utilization of rapid setting cements (e.g., calcium aluminate cement [45]), thermal curing [15], as well as the use of alternative activators and additives [46]. In essence, such alternate uses of pozzolans and activators can have a significant effect on the overall  $\text{CO}_2$  production and costs of the produced geopolymer concrete [47]. As noted by Ma et al. [48], the inclusion of a composite activator (e.g., sodium silicate with sodium sulfate) can reduce the overall  $\text{CO}_2$  production by at least 15–20%, while also significantly reducing the cost per MPa for a given geopolymer concrete section.

In that respect, in this study, two novel additives of sodium and magnesium sulfate that are naturally occurring minerals with formulas  $\text{Na}_2\text{SO}_4$  and  $\text{MgSO}_4$ , respectively, are used as additives to enhance the activation process. Although both chemical compounds are highly soluble in water, the pH of  $\text{Na}_2\text{SO}_4$  is reported to be approximately 8.5 [49], while  $\text{MgSO}_4$  has a lower pH of 6–7 [50]. Using lower pH activators can have major applications, such as the conservation of reactive metals and resins that do not react with encasing materials if the pH is not very high [51]. To date, however, very few studies have utilized naturally occurring sodium and magnesium sulfate as additives in geopolymer concrete. Rashad et al. [51], for instance, utilized sodium sulfate as a naturally occurring material to activate blast furnace slag. In their analysis, it was reported that the fineness of the precursor particles was more effective for the geopolymerization rate than increasing the sodium sulfate content. Rattanasak et al. [52] used sodium sulfate, among other additives, for its lower pH and reactivity to control the setting time of geopolymer concrete. It was reported that the presence of sodium sulfate retarded the leaching of silica and alumina from high-calcium coal fly ash (class C) and increased the setting time significantly. The reported results, however, showed an enhanced compressive strength later on. Ma et al. [48] reported that the addition of sodium sulfate could reduce the heat of geopolymerization due to its lower pH, and, thus, reduce the drying shrinkage of geopolymer specimens. Nonetheless, the addition of sodium sulfate has been reported to increase the overall content of microcracks. Qing-feng et al. [53] studied the microstructural properties of a coal fly ash-based geopolymer activated using sodium silicate and sodium sulfate. In their analysis, it was reported that only a higher content of sodium sulfate could cause a higher peak at the symmetrical stretching vibration of Si–O, Si–O–Si and Al–O–Si, which translated into promoting the formation of N–A–S–H gels. Jun and Oh [54] utilized sodium sulfate as an additive to coal fly ash (F)-based geopolymer concrete, and reported an enhanced strength development due to a change in pore size distribution. It was also reported that the addition of sodium sulfate resulted in higher strength values for lower Si/Al ratios of reaction products.

Although the aforementioned studies provided a significant contribution to alternate routes for the cleaner production of geopolymer concrete, the used precursors and activators in most of the mentioned studies were common coal fly ash and blast furnace slag, activated using a liquid sodium silicate [55] activator. To address this and practice an alternative route for the cleaner production of geopolymer binders, this study adopts the use of naturally occurring kaolin and raw ceramic powder, activated using potassium hydroxide (KOH), while sodium and magnesium sulfate are also added to evaluate their effectiveness on enhancing the activation process.

KOH is a strong base that is produced through the electrolysis of potassium chloride [56,57]. KOH is a major activator used in alkali-activated materials, and can be found in pellet, flake and powder forms [58]. The result of this study is found to be significant, and points to the potential application of sodium and magnesium sulfate to partially substitute commonly used activators for the production of greener geopolymer concretes. The following sections further elaborate on the experimental program of this study.

## 2. Experimental Program

### 2.1. Materials

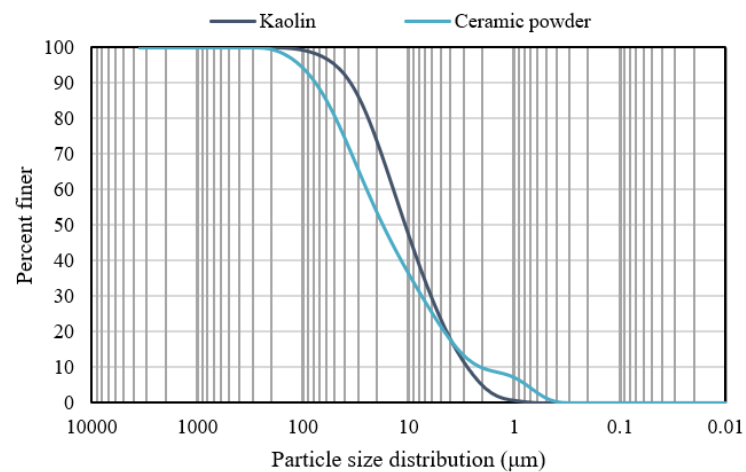
#### 2.1.1. Precursors

In this study, kaolin and ceramic powder with a  $\text{SiO}_2$  content of ~70% and 54% and a specific gravity of 2.53 and 2.72, respectively, were used as the main precursors. The specific surface areas of the ceramic and kaolin powders were obtained as  $2720 \text{ cm}^2/\text{g}$  and  $2530 \text{ cm}^2/\text{g}$ , respectively. Table 1 presents the results of an X-ray fluorescence (XRF) test conducted on the kaolin and ceramic powder based on mass percentage. In addition, a particle size analysis was also conducted on the kaolin and ceramic powder, the results of which are presented in Figure 1a. Figure 1b presents the X-ray diffraction (XRD) of the raw minerals. For this figure, the XRD analysis of raw materials was conducted using Bruker

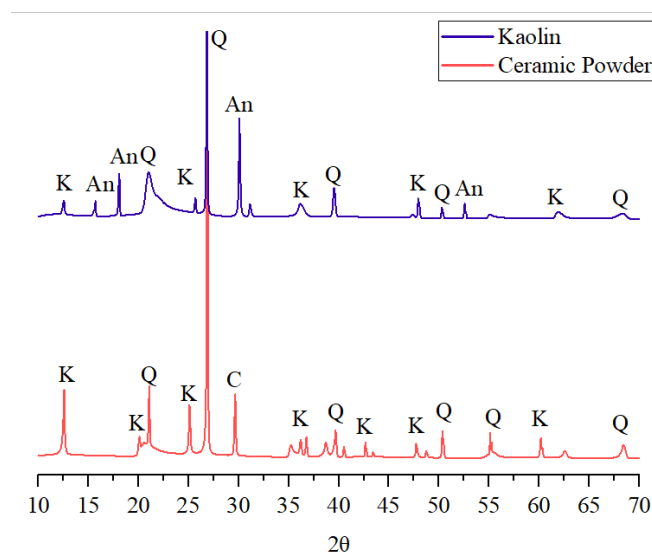
Phaser instruments with  $\text{CuK}\alpha$  radiation ( $\lambda = 1.542 \text{ \AA}$ ) at 40 kV. As shown in this figure, the major crystalline phases were quartz ( $\text{SiO}_2$ ) (PDF#01-083-2466), kaolinite ( $\text{Al}_2\text{Si}_2\text{O}_5(\text{OH})_4$ ) (PDF#01-072-2300) and anorthite ( $\text{CaAl}_2\text{Si}_2\text{O}_8$ ) (PDF#01-078-0432) in kaolin, while quartz, kaolinite and calcite ( $\text{CaCO}_3$ ) (PDF#01-072-1937) were observed in the ceramic powder, which was similar to that mentioned in Refs. [59–62].

**Table 1.** XRF of kaolin and ceramic powder.

Compound	Kaolin (%)	Ceramic Powder (%)
$\text{SiO}_2$	69.14	55.61
$\text{Al}_2\text{O}_3$	17.22	21.13
$\text{CaO}$	1.23	9.02
$\text{Fe}_2\text{O}_3$	0.46	0.88
$\text{MgO}$	0.28	0.31
$\text{SO}_3$	1.03	0.04
$\text{Na}_2\text{O}$	0.04	0.19
$\text{K}_2\text{O}$	0.65	0.76
$\text{P}_2\text{O}_5$	0.1	0.19



(a)



(b)

**Figure 1.** (a): Particle size analysis of kaolin and ceramic powder (CP); (b): XRD of raw kaolin and ceramic powder with: K—kaolinite; Q—quartz; C—calcite; An—anorthite.

### 2.1.2. Aggregate

A basalt aggregate with a specific gravity of  $2.74 \text{ g/cm}^3$  and a maximum size of 4 mm was used in this study. Figure 2 presents the sieve analysis (based on ASTM C136) conducted on the fine aggregate.

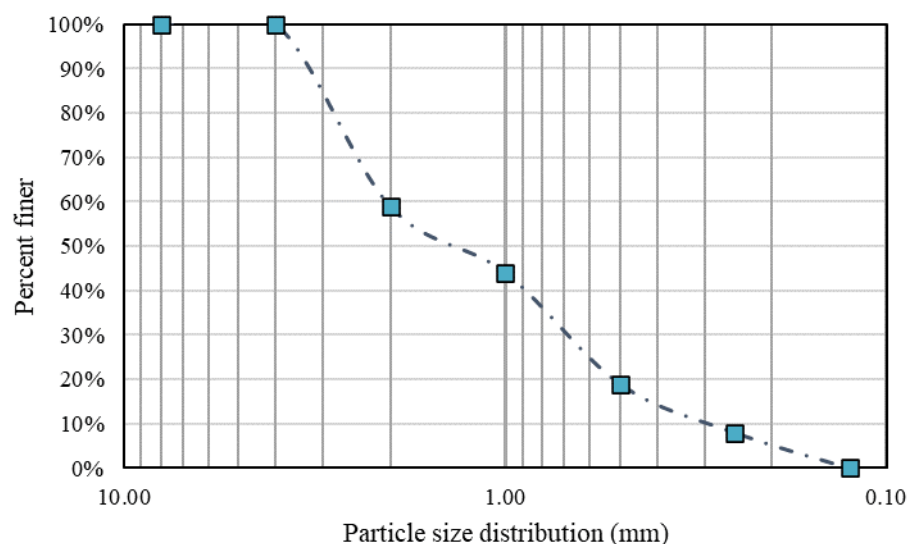


**Figure 2.** Particle size analysis of basalt aggregate.

### 2.1.3. Activator

To increase the alkalinity of the mixes, solid potassium hydroxide (KOH) with a molecular weight of  $56.11 \text{ g/mol}$  with a density of  $2.04 \text{ g/cm}^3$  was used. The ratio of KOH to binder was kept at 20% throughout all the mixes. Table 2 provides further information on the properties of the KOH used in this study.

**Table 2.** Properties of potassium hydroxide.

Potassium Hydroxide (KOH)	
Molecular weight	$56.11 \text{ g}\cdot\text{mol}^{-1}$
Density	$2.04 \text{ g}\cdot\text{cm}^{-3}$
Melting point	$406 \text{ }^\circ\text{C}$
Boiling point	$1320 \text{ }^\circ\text{C}$

## 2.2. Mix Proportions

In this study, a total of 28 mixes was prepared with a constant liquid-to-binder ratio of 0.5. In general, the liquid-to-binder ratio is a common term used in geopolymer binders, and it refers to the content of the activator to precursor. In the mixes, the kaolin content was replaced with ceramic powder at 0, 10, 20 and 30 vol.%. In the same way, sodium ( $\text{Na}_2\text{SO}_4$ ) and magnesium sulfate ( $\text{MgSO}_4$ ) were also added at 0, 3, 6 and 9 vol.%, substituting the kaolin content. The reason for the mentioned ratios was the authors' preliminary tests on the fresh properties of the mixes that led to choosing such specific ratios. Table 3 further shows the mix proportions used in this study. In this table, the mixes were labelled as follows: letters CP, NS and MS refer to ceramic powder, sodium and magnesium sulfate, respectively. The numbers following each letter indicate the content of each material used in the mix (% for sodium and magnesium sulfate and  $\text{kg/m}^3$  for the ceramic powder). For instance, CP30-NS9 represents a mix containing 30% ceramic powder and 9 vol% sodium sulfate.

Table 3. Mixture proportions.

Mixing Code	Ceramic Powder (kg/m <sup>3</sup> )	Kaolin (kg/m <sup>3</sup> )	Na <sub>2</sub> SO <sub>4</sub> (kg/m <sup>3</sup> )	MgSO <sub>4</sub> (kg/m <sup>3</sup> )	Aggregate (kg/m <sup>3</sup> )	K*/Binder (%)	Liquid/Binder
CP0	0	450	0	0	1350	20	0.5
CP0-NS3	0	436.5	13.5	0	1350	20	0.5
CP0-NS6	0	423	27	0	1350	20	0.5
CP0-NS9	0	409.5	40.5	0	1350	20	0.5
CP10	45	405	0	0	1350	20	0.5
CP10-NS3	45	391.5	13.5	0	1350	20	0.5
CP10-NS6	45	378	27	0	1350	20	0.5
CP10-NS9	45	364.5	40.5	0	1350	20	0.5
CP20	90	360	0	0	1350	20	0.5
CP20-NS3	90	346.5	13.5	0	1350	20	0.5
CP20-NS6	90	333	27	0	1350	20	0.5
CP20-NS9	90	319.5	40.5	0	1350	20	0.5
CP30	135	315	0	0	1350	20	0.5
CP30-NS3	135	301.5	13.5	0	1350	20	0.5
CP30-NS6	135	288	27	0	1350	20	0.5
CP30-NS9	135	274.5	40.5	0	1350	20	0.5
CP0-MS3	0	436.5	0	13.5	1350	20	0.5
CP0-MS6	0	423	0	27	1350	20	0.5
CP0-MS9	0	409.5	0	40.5	1350	20	0.5
CP10-MS3	45	391.5	0	13.5	1350	20	0.5
CP10-MS6	45	378	0	27	1350	20	0.5
CP10-MS9	45	364.5	0	40.5	1350	20	0.5
CP20-MS3	90	346.5	0	13.5	1350	20	0.5
CP20-MS6	90	333	0	27	1350	20	0.5
CP20-MS9	90	319.5	0	40.5	1350	20	0.5
CP30-MS3	135	301.5	0	13.5	1350	20	0.5
CP30-MS6	135	288	0	27	1350	20	0.5
CP30-MS9	135	274.5	0	40.5	1350	20	0.5

\*: K: potassium hydroxide.

### 2.3. Specimen Preparation and Test Methods

In this study, geopolymer mortar samples were prepared by placing the freshly mixed materials in proper molds and then into an oven with a constant temperature of 115 °C for 24 h. Finally, the samples were removed from the oven and kept in ambient temperature until tested. Figure 3 presents the detailed mixing procedure used in this study.

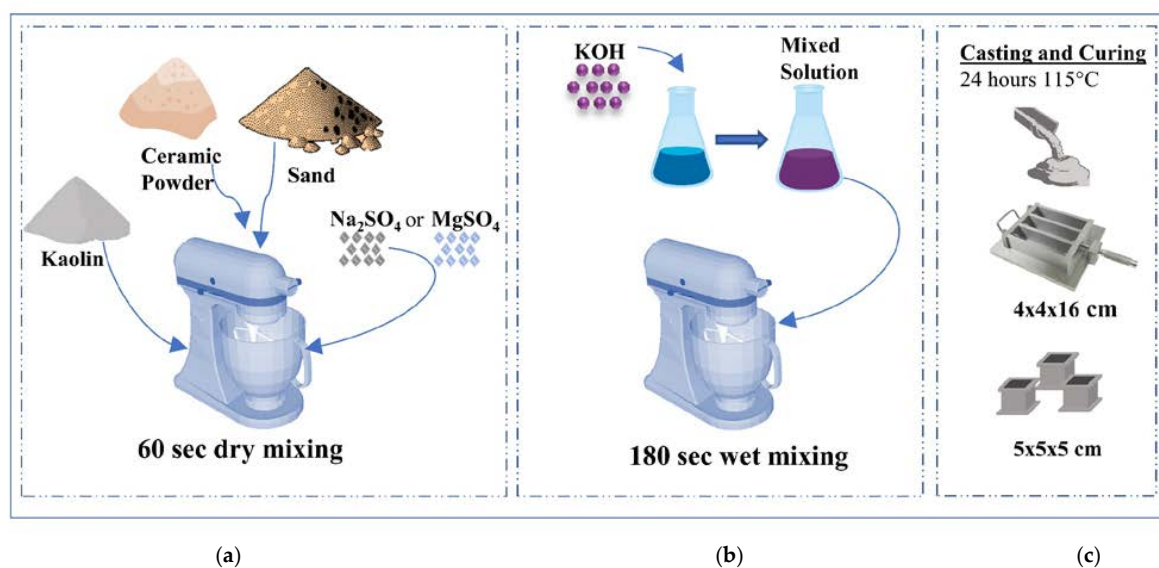


Figure 3. Mixing procedure used in this study with (a) initial dry mixing (b), including solutions and (c) casting and curing of the produced specimens.



To analyze the mechanical properties of the mixes, after 28 days of curing, compressive and flexural strength tests were conducted by using  $40 \times 40 \times 160$  mm samples based on EN 1015-11 [63]. In that respect, three specimens were created for each flexural strength test. The compressive test was applied on 6 half samples obtained from the flexural test. In addition, to assess the physical properties of the produced geopolymer samples, dry bulk density, porosity and water absorption tests were conducted on specimens in accordance to ASTM C642-13 [64]. The dry bulk density, porosity and water absorption of the produced mortars were calculated with Equations (1)–(3), respectively, where the mass of the oven-dried sample was represented with  $A$ . The surface-dry sample mass after immersion and immersion-boiling is represented by  $B$  and  $C$ , respectively.  $D$  represents the mass of the sample in water. Additionally, the term  $\rho$  refers to the density of water.

$$\text{Dry bulk density (\%)} = \left( \frac{A}{C - D} \right) \times \rho \quad (1)$$

$$\text{Porosity (\%)} = \left( \frac{C - A}{C - D} \right) \times 100 \quad (2)$$

$$\text{Water absorption (\%)} = \left( \frac{B - A}{A} \right) \times 100 \quad (3)$$

In conjunction, ultrasonic pulse velocity (UPV) as a nondestructive testing (NDT) method was performed to control the level of uniformity of the samples. X-ray powder diffraction (XRD) was employed to characterize the crystalline phases of the raw materials and produced geopolymers. To evaluate the produced geopolymer chemical bonds and stability, a spectroscopic investigation was carried out using a Fourier transform infrared (FTIR) spectrometer (Shimadzu IRSpirit model) over a spectrum range of  $4000\text{--}400\text{ cm}^{-1}$ . The microstructures and surface morphologies of the specimens were obtained with scanning electron microscopy (SEM, TESCAN MAIA3 XMUV). The elemental distribution of hydration products was analyzed with energy-dispersive X-ray spectroscopy (EDS).

### 3. Results and Discussion

#### 3.1. Compressive and Flexural Strength

Figure 4a,b represents the 28-day compressive strength of the geopolymer mortars according to the  $\text{Na}_2\text{SO}_4$  or  $\text{MgSO}_4$  contents (0%, 3%, 6% and 9%), with the replacement of 10%, 20% and 30% of kaolin with ceramic powder. At 0%  $\text{Na}_2\text{SO}_4$  and  $\text{MgSO}_4$  content, the increase in ceramic powder content from 0% to 10 and 20 wt.% increased the compressive strength from 6.5 to 7.9 and 11.5 MPa, respectively. This finding could be explained by the fact that ceramic powder has a higher specific surface area than kaolin, creating a denser matrix composition. Moreover, Xu et al. [65] reported in a study on using natural aluminosilicate materials to synthesize geopolymers that the rate of Al separation from low-reactivity kaolin is mostly insufficient to create a gel formation. In this regard, it requires extra time for interactions among raw materials due to the weak reactivity of kaolinite. However, using low-reactivity kaolinite solely does not create a good synergy between the aluminosilicate sources, leading to the formation of a poor structure [65]. In parallel with this finding, the increase in the content of ceramic powder supports gel formation, as it increases the amount of kaolinite and other aluminosilicates simultaneously, effectively improving the compressive strength of the material. The results demonstrated that the substitution of 20 wt.% ceramic powder decreased the compressive strength by 5%. This reduction might be explained due to the use of ceramic powder above 20 wt%, lowering the polymerization reaction and not contributing to the strength values. The increased ceramic powder content reduced the amount of  $\text{SiO}_2$  in the total binder, which caused a decrease in the compressive strength.

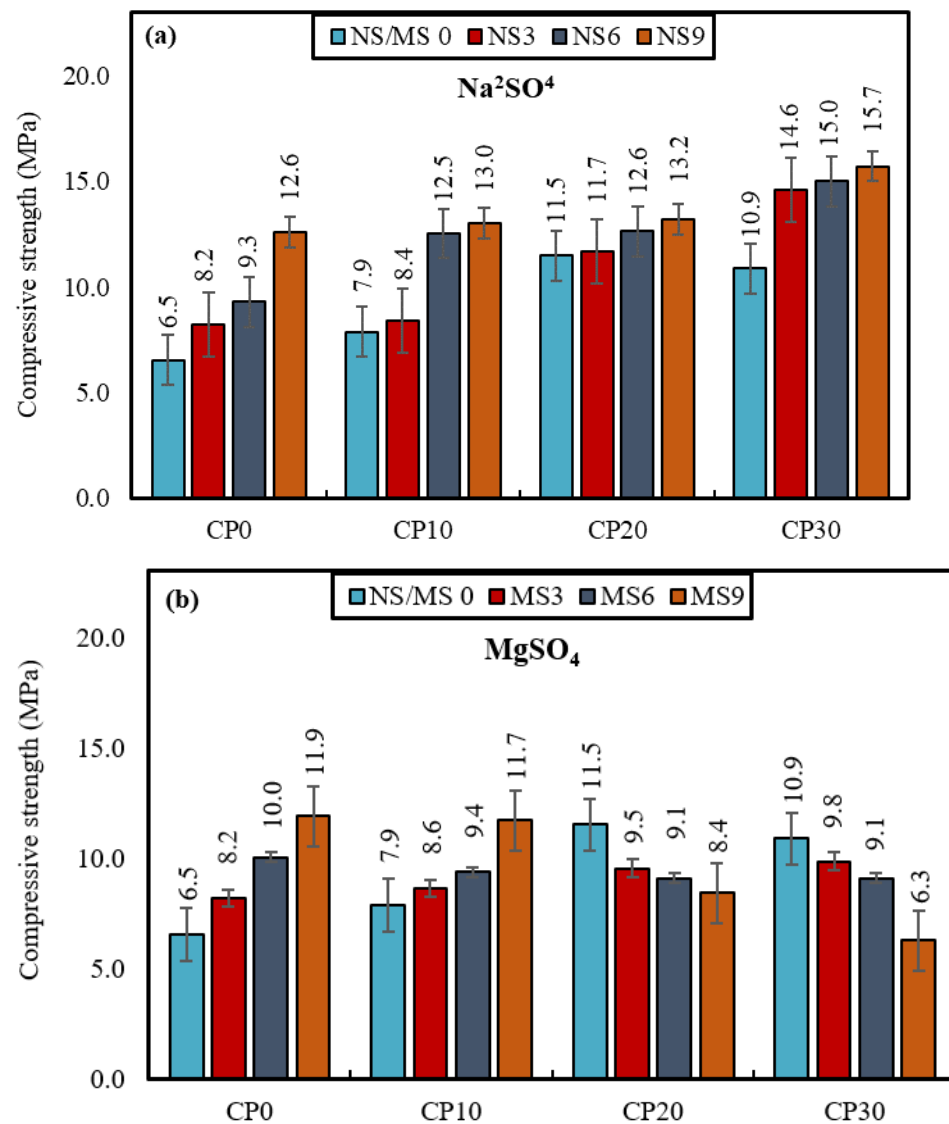


**Figure 4.** Compressive strength of mixes after 28 days of curing for mixes produced (a) with Na<sub>2</sub>SO<sub>4</sub> and (b) with MgSO<sub>4</sub>.

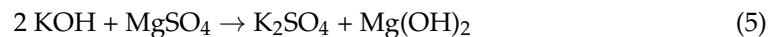
In the Na<sub>2</sub>SO<sub>4</sub> introduced groups, the compressive strength rose gradually when increasing the replacement levels of kaolin with ceramic powder. Based on the obtained test results, it was clearly seen that the addition of Na<sub>2</sub>SO<sub>4</sub> increased the compressive strength of the specimens regardless of the ceramic powder content, and the highest compressive strength was obtained as 15.7 MPa in the sample with 9% Na<sub>2</sub>SO<sub>4</sub> and 30% ceramic powder. These results may be similar to the results obtained in sodium-silicate-activated fly ash-based geopolymer containing various proportions of sodium sulfate in Ref. [53]. Qing-feng et al. reported that the acceptable introduction of Na<sub>2</sub>SO<sub>4</sub> significantly increased the strength of the geopolymers, as it highly promoted geopolymerization [53]. With the usage of higher amounts of Na<sub>2</sub>SO<sub>4</sub>, the dissolution rate of aluminosilicates increased considerably, and the formation of N-A-S-H gel was accelerated [53]. Consequently, the occupation of Na<sub>2</sub>SO<sub>4</sub> in geopolymer systems is advantageous for developing compressive strength values, which is parallel with the results of the current study. In Equation 1, the reaction products of Na<sub>2</sub>SO<sub>4</sub> and KOH were given. As a result of the reaction, the presence of additional NaOH was witnessed in the medium. It is known that K<sub>2</sub>SO<sub>4</sub> can also be



used as an activator [66].  $K_2SO_4$  and the additional NaOH released during the reaction was also effective in increasing the compressive strength.



Although the increase in the amount of  $MgSO_4$  (from 0% to 9%) for the mortars with a 0% and 10% content of ceramic powder remarkably increased the compressive strength values by 88% and 48%, it gradually reduced the strength values of those with a 20% and 30% content of ceramic powder by approximately 25% and 42%, respectively. In samples with  $MgSO_4$ , while the mortar with 0% ceramic powder and 9%  $MgSO_4$  (CP0MS9) had the highest compressive strength value of 11.91 MPa, the lowest value was determined as 6.3 MPa in the mortar containing 30% ceramic powder with 9%  $MgSO_4$  (CP30MS9). A study conducted by Kang et al. [67] using various contents (2, 4, 6, 8 and 10%) of  $MgSO_4$  as the activator in slag-based geopolymer paste showed an explicit reduction of almost 50% in compressive strength with the increase in the amount of  $MgSO_4$  from 6% to 10%. This finding was attributed to the lower activation effect of  $MgSO_4$ , leading to the formation of a porous structure, significantly decreasing the compressive strength. Moreover, it was reported that lower pH environments ( $\text{pH} < 11.5$ ) lowered the compressive strength values because of the inadequate activation of slags [52,67]. In parallel with the results of this study, the addition of higher amounts of  $MgSO_4$  deteriorated the compressive strength, as it remarkably reduced the pH of the environment. In general, the compressive strength test results revealed that the addition of  $Na_2SO_4$  significantly improved the compressive strength, while the addition of  $MgSO_4$  did not show a similar trend. In Equation (2), the reaction products of  $MgSO_4$  and KOH were given. It could be seen that the additional  $Mg(OH)_2$  and  $K_2SO_4$  were formed as a result of the reaction.  $Mg(OH)_2$  is the aqueous form of MgO. It was stated that the MgO additive in geopolymer concrete can increase the compressive strength [68]. The type and amount of the activator are effective in increasing and decreasing the compressive strength [69,70]. Therefore, the compressive strength of the samples containing  $MgSO_4$  did not increase significantly.



The flexural strength of the geopolymer mortars was investigated at 28 days, and the effect of various contents of  $Na_2SO_4$ ,  $MgSO_4$  and ceramic powder is presented in Figure 5a,b. Similar to the overall trend witnessed in compressive strength, the addition of ceramic powder to the mixtures without salts remarkably increased the geopolymer mortars' flexural strengths. The introduction of ceramic powder from a 0 to 30% replacement level almost doubled the flexural strength values (1.23 to 2.40 MPa). The increase in the flexural strength might have been attributed to the ceramic powder's higher specific surface area, saturating the geopolymer matrix's pores and improving the interface zone that strengthened the bonding to maintain the flexural loading. Furthermore, the incorporation of  $Na_2SO_4$  into the geopolymer mixtures remarkably developed the flexural strength, owing to the contribution of  $Na_2SO_4$  to the geopolymerization reaction, regardless of the utilization of ceramic powder [53]. The increase in flexural strength was found to be 56 and 117% with an increasing  $Na_2SO_4$  content from 0 to 3 and 9%, respectively. However, the effect of the  $MgSO_4$  increase on the flexural strength did not show a clear trend, as seen in the  $Na_2SO_4$  addition. The addition of  $MgSO_4$  (0 to 9%) on the mixes incorporating 0% and 10% ceramic powder increases the flexural strength values by almost 95% and 70%, respectively. However, the  $MgSO_4$  addition to the specimens, including ceramic powder of above 10 wt.%, adversely affected the flexural strength values. Similar to the compressive strength test results, this reduction was due to the fact that the addition of  $MgSO_4$  decelerated the geopolymerization by lowering the ambient pH and preventing the formation of gels.

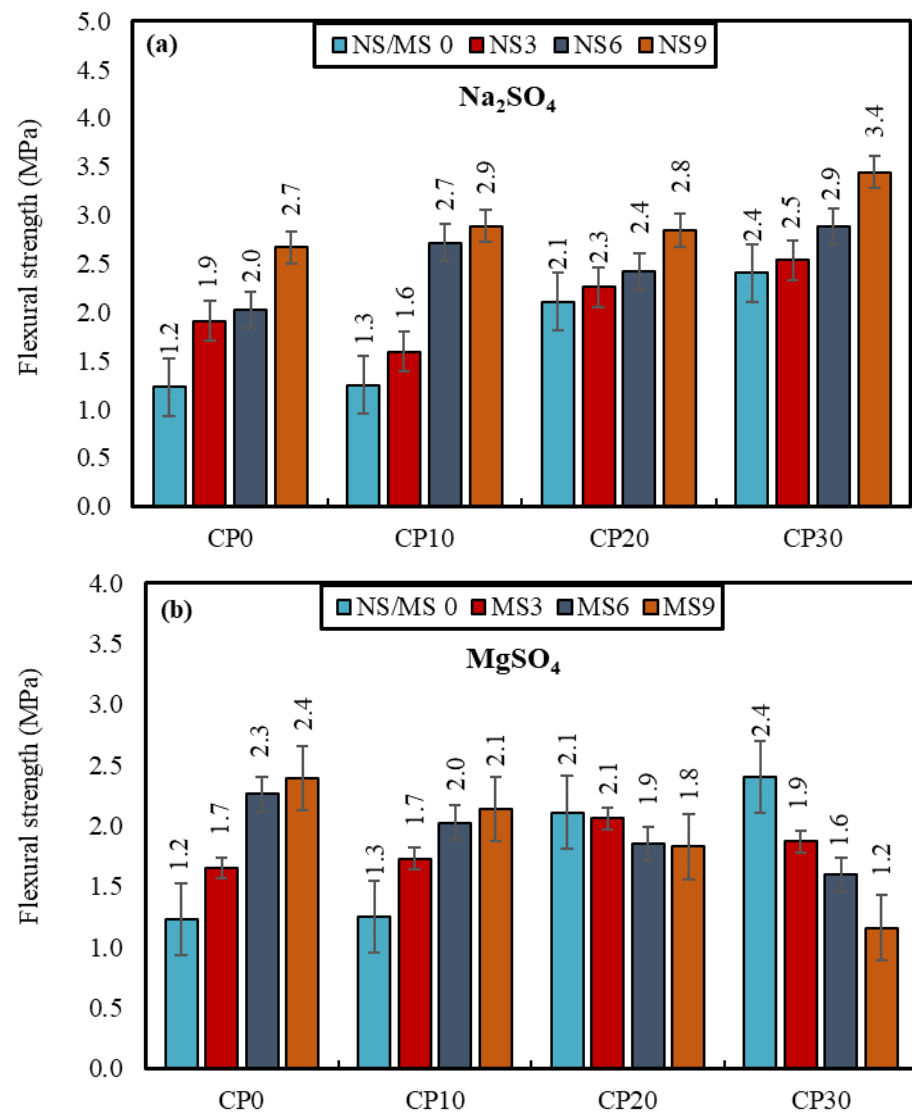


**Figure 5.** Flexural strength of mixes after 28 days of curing for mixes produced (a) with  $\text{Na}_2\text{SO}_4$  and (b) with  $\text{MgSO}_4$ .

### 3.2. Dry Unit Weight

Figure 6a,b plot the dry unit weight of the geopolymer samples, ranging between  $2.02 \text{ g/cm}^3$  and  $2.13 \text{ g/cm}^3$ . In the specimens with 0%  $\text{Na}_2\text{SO}_4$  and  $\text{MgSO}_4$ , the increase in the ceramic powder content from 0% to 10%, 20% and 30 wt.% enhanced the unit weight from  $2.03$  to  $2.05$ ,  $2.07$  and  $2.12 \text{ g/cm}^3$ , respectively. The ceramic powder's surface area of reaction was higher than kaolin's ( $2720 \text{ cm}^2/\text{g}$  and  $2530 \text{ cm}^2/\text{g}$ , respectively), leading to the formation of a denser matrix and with a higher unit weight. In addition, the unit weight of samples containing  $\text{Na}_2\text{SO}_4$  varied from  $2.05$  to  $2.13 \text{ g/cm}^3$ , while it ranged between  $2.02$  and  $2.07 \text{ g/cm}^3$  for specimens incorporating  $\text{MgSO}_4$ . The highest unit weight was obtained for the mixture incorporating the combined use of 30% ceramic powder and 9%  $\text{Na}_2\text{SO}_4$  (CP30NS9) at  $2.13 \text{ g/cm}^3$ . The geopolymer specimens with 0%  $\text{MgSO}_4$  revealed a growing trend in the unit weight value, with a rise in ceramic powder or  $\text{Na}_2\text{SO}_4$  content. However, this variation was less prominent in the series containing  $\text{MgSO}_4$ . The lowest of unit weights was obtained for the mixture containing 30% ceramic powder and 9%  $\text{MgSO}_4$  (CP30MS9) at  $2.02 \text{ g/cm}^3$ .

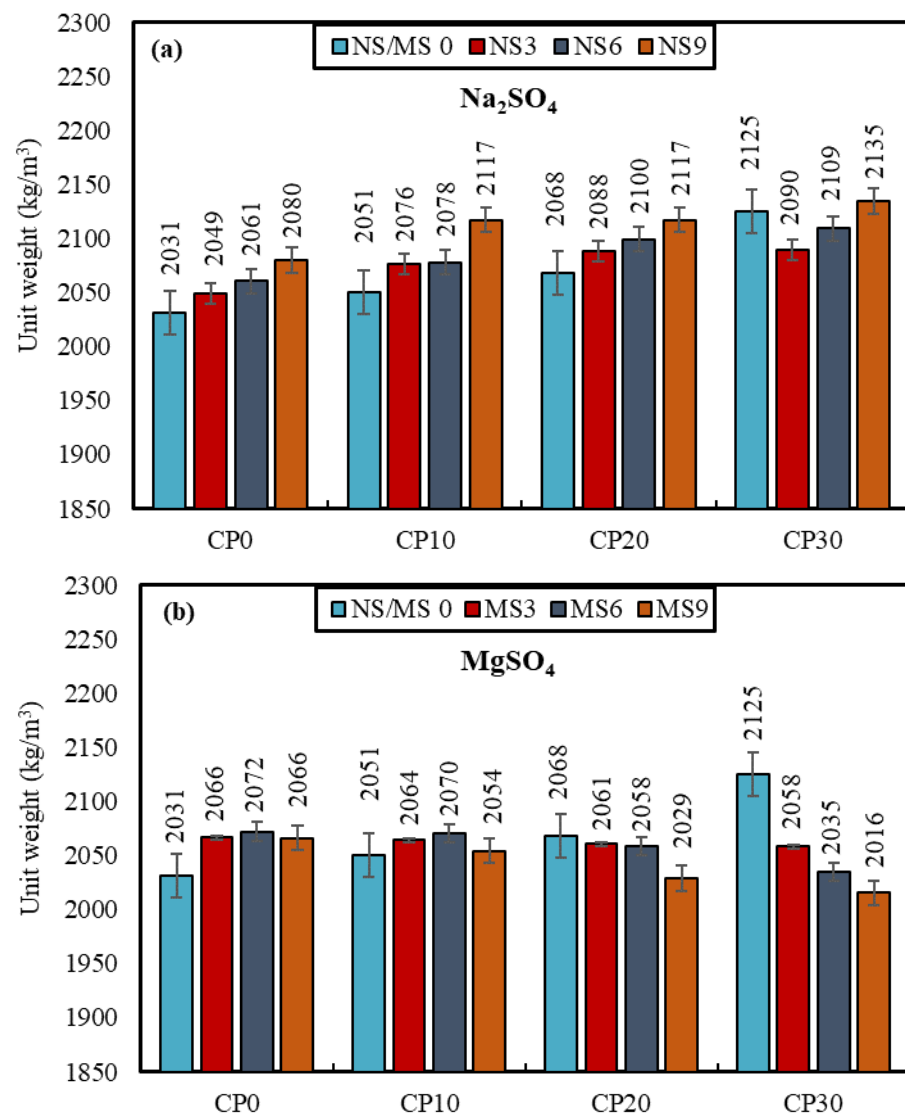


**Figure 6.** Dry bulk density (unit weight) of mixtures for mixes produced (a) with Na<sub>2</sub>SO<sub>4</sub> and (b) with MgSO<sub>4</sub>.

### 3.3. Porosity and Water Absorption

Test results revealed that the porosity of mortars without salts decreased with an increased ceramic powder content, which could be attributed to the higher specific surface area of ceramic powder than kaolin (see Figure 7a,b). To illustrate, the increase in the amount of ceramic powder from 0% to 30% reduced the porosity by 38%. In cases where Na<sub>2</sub>SO<sub>4</sub> was introduced, the highest porosity of 12% was obtained in the series with 3% Na<sub>2</sub>SO<sub>4</sub> and 0% ceramic powder (CP0NS3), while the lowest porosity was observed in the mortar containing 30% ceramic powder and 9% Na<sub>2</sub>SO<sub>4</sub> (CP30NS9). The results clearly showed that the addition of Na<sub>2</sub>SO<sub>4</sub> played a critical role in reducing the porous structure of the mortars. The highest porosity was found in the sample with 30% ceramic powder and 9% MgSO<sub>4</sub> (CP30MS9), while the lowest porosity was found in the specimen with 6% MgSO<sub>4</sub> and 10% ceramic powder (CP10MS6) as 13.3% and 9.8%, respectively. According to the results obtained from previous studies, it was reported that aluminosilicate hydrate gels show less formation in environments where the pH is lower than 9.5 [71,72]. For this reason, it is inevitable to obtain a high porosity and low compressive strength in lower pH environments. Therefore, the utilization of supplementary materials with a lower pH (<9.5), such as MgSO<sub>4</sub>, causes the formation of a porous matrix, remarkably reducing the mechanical performance [67].

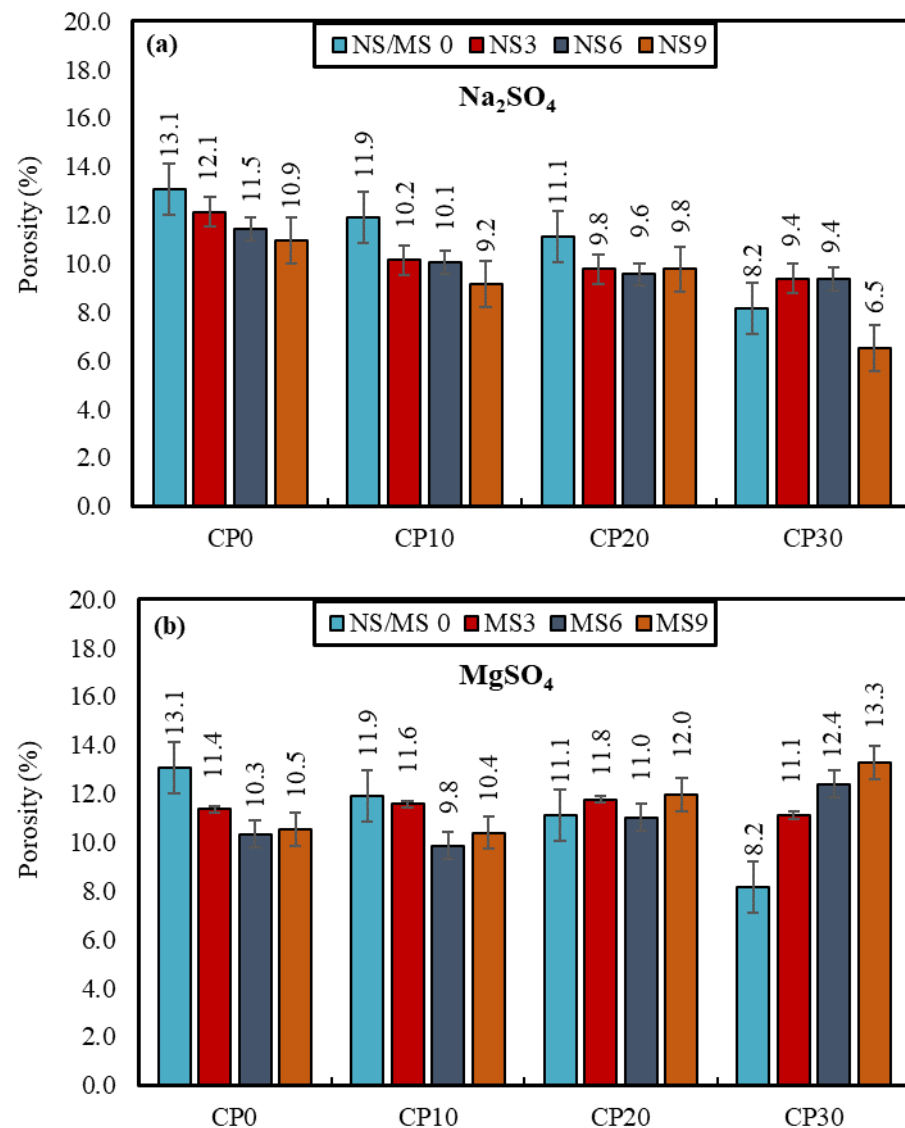


**Figure 7.** Porosity of various mixes after 28 days of curing for mixes produced (a) with  $\text{Na}_2\text{SO}_4$  and (b) with  $\text{MgSO}_4$ .

The water absorption test results are displayed in Figure 8a,b. The pore-filling effect of the ceramic powder was more pronounced in specimens without  $\text{Na}_2\text{SO}_4$  and  $\text{MgSO}_4$ , in which the water absorption reduced from 6.34% in CP0 to 3.86% in CP30. In addition, the mortars containing a higher kaolin content were found to demand a higher amount of water because of the characteristics of the material, being an uncalcined clay and capable of absorbing considerable amounts of water [73]. While the water absorption of the mortars incorporating  $\text{Na}_2\text{SO}_4$  ranged between 3.16% and 6.34%, the values fluctuated between 4.78% and 6.62% for those with  $\text{MgSO}_4$ . The specimen with 9%  $\text{Na}_2\text{SO}_4$  and 30% of ceramic powder (CP30NS9) revealed the lowest level of water absorption at 3.2%, which clearly exhibited the effect of  $\text{Na}_2\text{SO}_4$  on the water absorption characteristics of the geopolymers. It might have also been attributed to the reaction between  $\text{Na}_2\text{SO}_4$  and the existing alkali activators, reducing the void ratio.

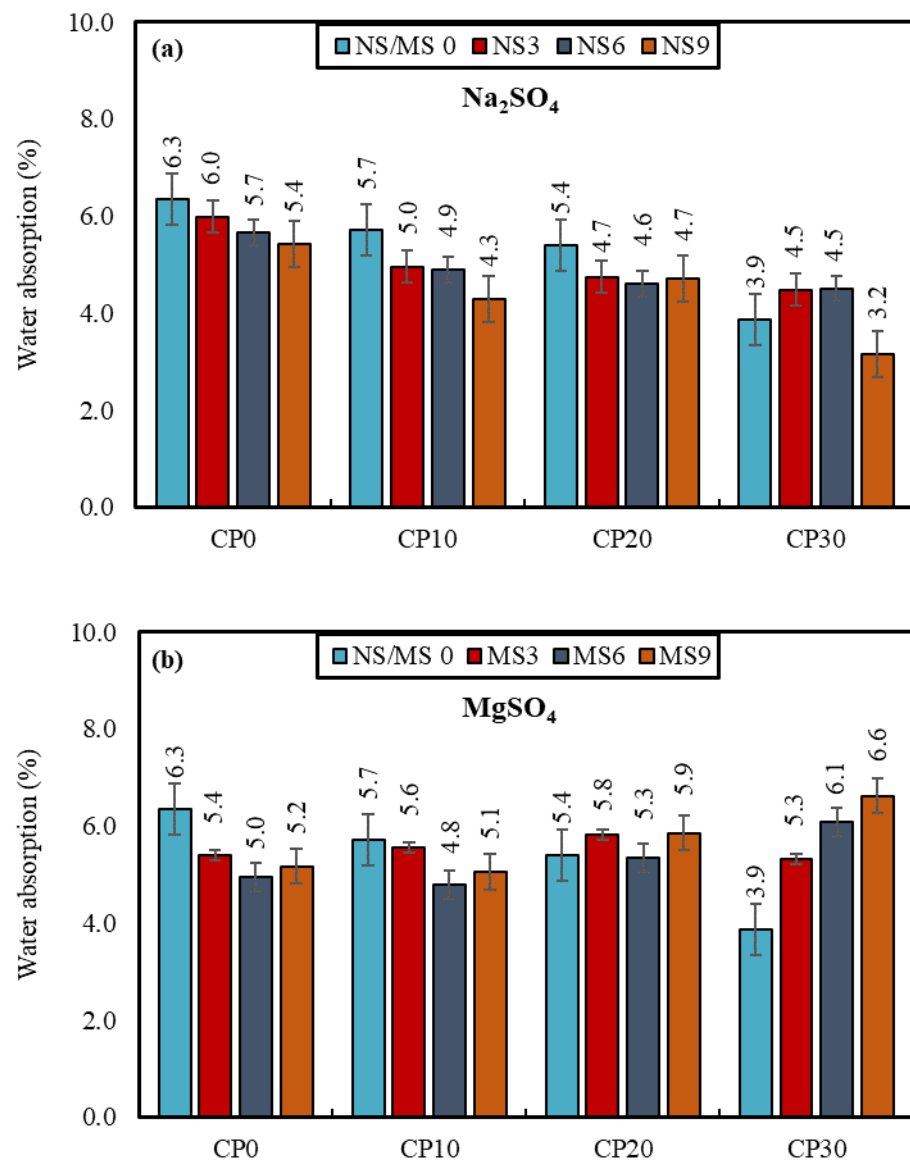


**Figure 8.** Water absorption of various mixes after 28 days of curing for mixes produced (a) with  $\text{Na}_2\text{SO}_4$  and (b) with  $\text{MgSO}_4$ .

On the other hand, the addition of  $\text{MgSO}_4$  (0 to 9%) reduced the water absorption of mortars with 0 and 10% of ceramic powder, while it did not positively affect the water absorption of geopolymers containing 20% and 30% of ceramic powder. To demonstrate, the increase in the amount of  $\text{MgSO}_4$  (0 to 9%) decreased the water absorption of CP0 and CP10 by 22% and 12%; however, it increased the water absorption of CP20 and CP30 by 10% and 70%, respectively. As mentioned earlier,  $\text{MgSO}_4$  created a porous matrix due to the lower pH [67], increasing water absorption in series containing  $\text{MgSO}_4$  at higher ratios. Consequently,  $\text{Na}_2\text{SO}_4$  played a more influential role in water absorption characteristics of geopolymers than  $\text{MgSO}_4$ .

Figure 9 plots the relations between the porosity, water absorption and dry unit weight of the geopolymer mortars. Rather linear relations between the porosity and water absorption and between the porosity and dry unit weight were determined, with 0.99 and 0.85 coefficients of correlation, respectively.

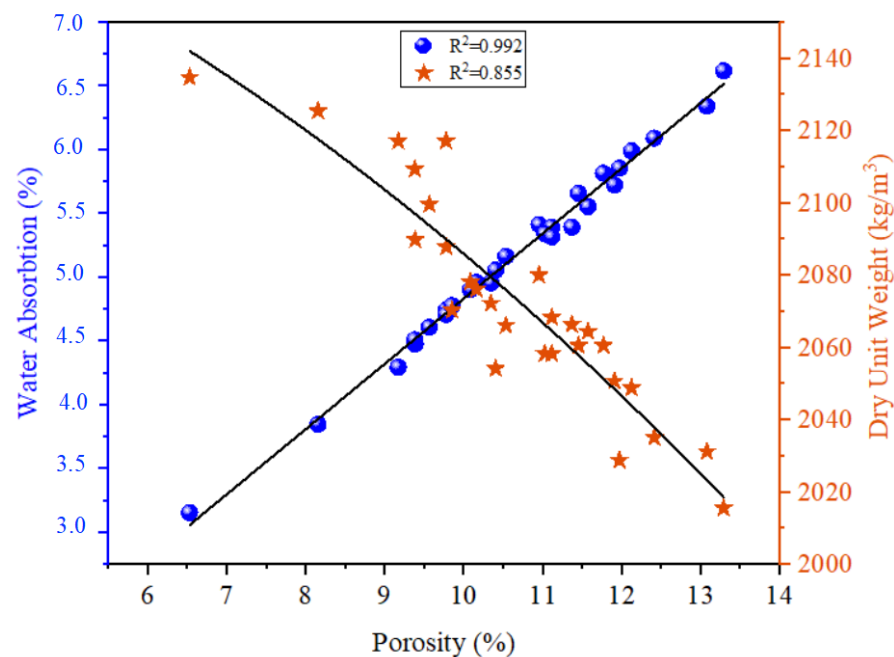


**Figure 9.** Correlation of porosity vs. water absorption and dry unit weight.

### 3.4. Ultrasound Pulse Velocity

The ultrasonic pulse velocity (UPV) test was employed to evaluate the internal conditions of the concrete nondestructively [74]. The mean velocity of the ultrasonic pulse in the geopolymer mortars measured after 28 days of curing is plotted in Figure 10a,b. Based on the test results, in mixes without  $\text{Na}_2\text{SO}_4$  and  $\text{MgSO}_4$ , the increased level of ceramic powder was found to increase the UPV results of the mortars. This was believed to have been caused by higher compaction due to the pore-filling effect of the ceramic powder. In detail, the UPV value of CP0 was measured as 1697 m/s, while that of CP30 was measured as 2102 m/s. This showed a ~19% increase in the UPV value when 30% of ceramic powder was used to substitute the kaolin. Similarly, since the addition of  $\text{Na}_2\text{SO}_4$  supported the geopolymerization reaction, its contribution to the compressive strength was also supported by the UPV results. To illustrate, an increase in the  $\text{Na}_2\text{SO}_4$  content from 0 to 9% enhanced the UPV value of the specimen without ceramic powder from 1696 to 1992 m/s. The improved UPV findings could be attributed to the formation of a denser structure in the geopolymer mortar matrix [75].

Although the addition of  $\text{MgSO}_4$  (0 to 9%) in the specimens with 0% and 10% ceramic powder slightly increased the UPV values by 14% and 9%, it reduced the UPV values in the samples with 20% and 30% ceramic powder by almost 15% and 30%, respectively. This reduction could be explained by the fact that a higher ceramic powder content did not contribute to geopolymerization, and the excessive utilization of  $\text{MgSO}_4$  reduced the mix's pH, resulting in a lower reaction. The trend was similar to the compressive strength test results reported in Section 3.1.

A linear regression approach was implemented to establish the correlation of UPV and the unit weight of geopolymer mortars, and the results were plotted in Figure 11. As can be seen, a linear relationship was witnessed among the unit weight and UPV values with reasonable confidence for the correlation factor ( $R^2$ ) of 0.89. The influence of supplementing ceramic powder and/or  $\text{Na}_2\text{SO}_4$  in geopolymers was evident on the velocity of the ultrasonic pulse and its respective relationship with the unit weight values. This showed an overall improvement, which may be owed to the formation of a denser matrix when ceramic powder or  $\text{Na}_2\text{SO}_4$  were added. Based on the figure, the higher reactivity of the ceramic powder and  $\text{Na}_2\text{SO}_4$  accelerated geopolymerization and led to a more consolidated and robust composition.



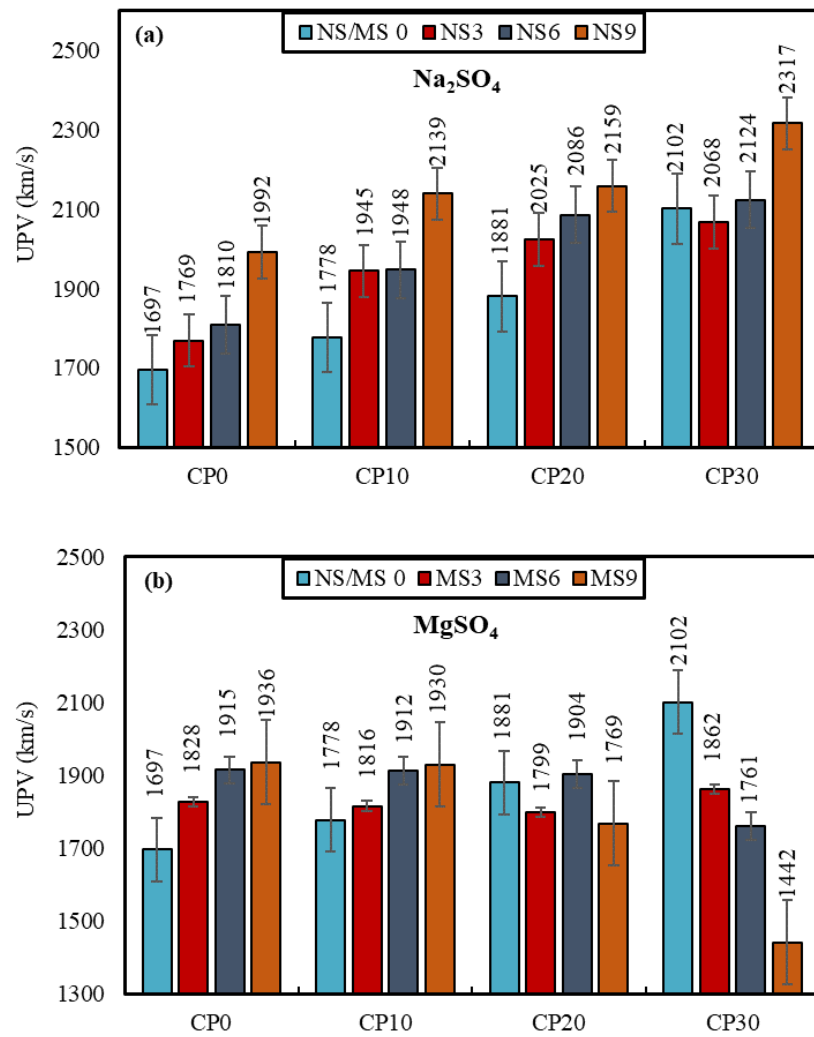


**Figure 10.** UPV of various mixes after 28 days of curing for mixes produced (a) with  $\text{Na}_2\text{SO}_4$  and (b) with  $\text{MgSO}_4$ .

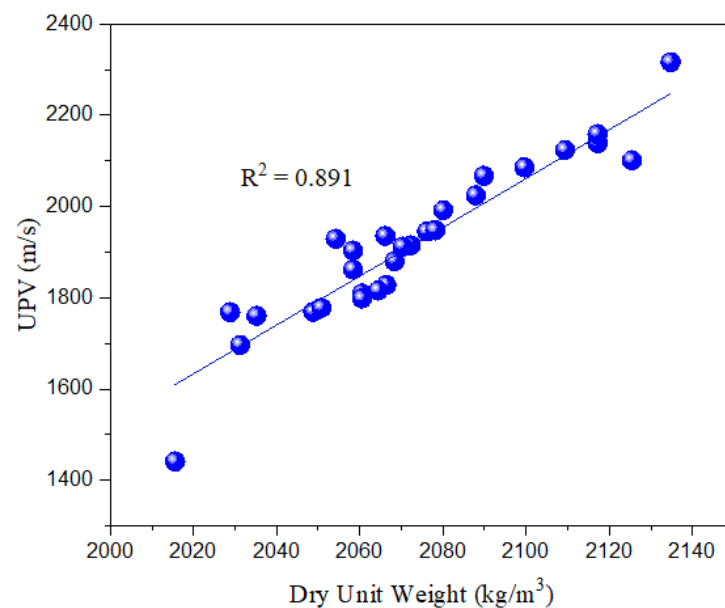


**Figure 11.** Correlation of UPV and unit weight.

### 3.5. Microstructural Analysis

#### 3.5.1. X-ray Diffraction (XRD)

Figure 12 presents the XRD patterns of the selected mixtures characterized at 28 days. The XRD patterns of CP0 and CP30 revealed the presence of quartz and kaolinite, earlier recognized as chief minerals in raw kaolin and ceramic powder. The XRD spectrum of CP0 showed the intense phase of quartz, with reasonably intense peaks of kaolinite and muscovite, roughly similar to those witnessed in raw kaolin (see Figure 1b). However, the patterns of CP30 exhibited a decrease in the intensity of quartz, especially at approximately  $26.5^\circ$  ( $2\theta$ ). This finding could be explained by the increase in the amount of ceramic powder; significant parts of the crystalline structures were spent during the geopolymerization, producing an amorphous or semicrystalline structure and developing a compressive strength of composition [76,77]. Furthermore, various amounts of anorthite ( $\text{CaAl}_2\text{Si}_2\text{O}_8$ ), which is a calcium-based mineral in the feldspar group derived only from a ceramic powder precursor, phases resided in CP30.

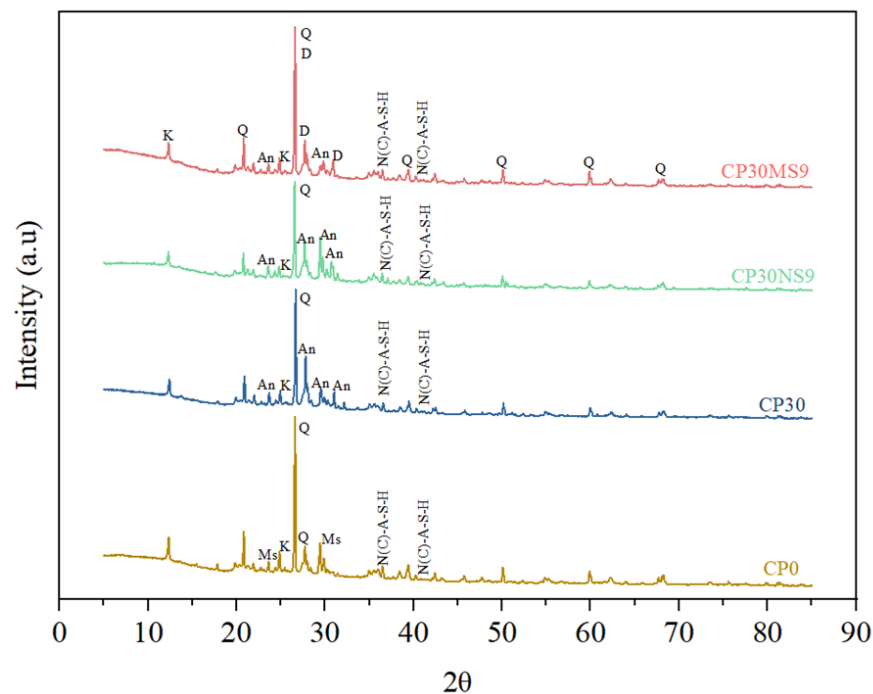


**Figure 12.** XRD patterns of geopolymers. K—kaolinite; Q—quartz; Ms—muscovite; An—anorthite; D—diopside.

The XRD spectra of the geopolymers incorporating  $\text{Na}_2\text{SO}_4$  (CP30NS9) and  $\text{MgSO}_4$  (CP30MS9) were also presented in Figure 12. Based on CP30NS9, the presence of low-concentration peaks of kaolinite, moderate-intensity peaks of anorthite with the intense phase of quartz could be seen. The intense peak of anorthite phases exhibited a slight decrease in CP30NS9 than CP30. This indicated that the addition of  $\text{Na}_2\text{SO}_4$  could dissolve part of the crystalline phase and convert it into a semicrystalline geopolymer gel. In line with the compressive strength results (see Figure 4), the XRD patterns of CP30NS9 presented the lowest intensity of quartz, followed by CP30 and CP0, respectively. For CP9NS9,  $\text{Na}_2\text{SO}_4$  did not lead to the formation of a different crystalline phase in the geopolymers. An intense peak of sodium sulfate was not obtained on the diffractogram, showing that  $\text{Na}_2\text{SO}_4$  reacted almost entirely in the geopolymer system. The study conducted by Qing-feng determined that there was no sodium sulfate peak in the geopolymer with a low salt content [53]. On the other hand, the introduction of  $\text{MgSO}_4$  into the geopolymers resulted in boosted peaks of quartz compared to other mixes, indicating the lower utilization of these crystalline forms throughout the reaction processes of CP30MS9, causing an important

reduction in the compressive strength of the geopolymers. With the addition of  $\text{MgSO}_4$  to the geopolymers, the anorthite peaks at approximately  $23.5^\circ$ ,  $27.6^\circ$  and  $30.7^\circ$   $2\theta$  were replaced with diopside ( $\text{CaMgSi}_2\text{O}_6$ ). N(C)-A-S-H gel (geopolymer gel) was observed at approximately  $37^\circ$  and  $41^\circ$   $2\theta$  in the XRD patterns of all produced samples with different intensities. The increase in this gel resulted in an increase in strength values [78–81].

### 3.5.2. FTIR

The result of the FTIR test is presented in Figure 13. It can be seen in Figure 13a that, for most of the mixes, two broad absorbance bands at approximately 450–1000 and 3600–3700  $\text{cm}^{-1}$  were observable. According to Ref. [82], the asymmetric stretching from 950 to 1200 was the result of the Si–O–Si and Al–O–Si vibrational bands. Ref. [30] noted that the bands at approximately 3600 corresponded to the O–H stretching that reflected the presence of structural water. It can be seen from Figure 13a that the inclusion of 30% of ceramic powder slightly reduced the transmittance of the two bands at 3688 and 1001. Based on Ref. [30], this small shift to a lower frequency was associated with the penetration of  $\text{Al}^{4+}$  (tetrahedral aluminum atoms) into the reacting binder system.

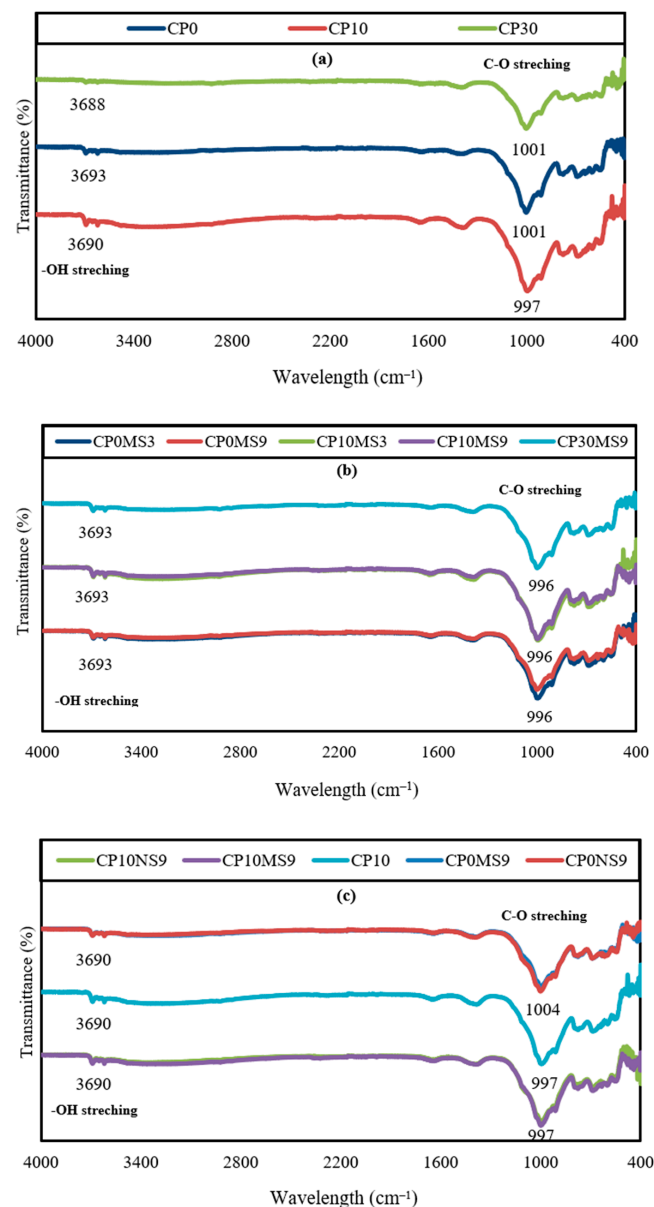
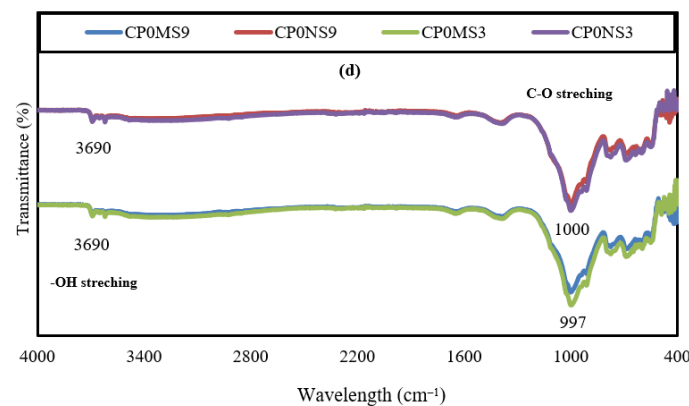


Figure 13. Cont.



**Figure 13.** FTIR result of mixes containing ceramic powder, magnesium and sodium sulfate with (a) mixes containing only CP (b) mixes produced with CP and MS (c) mixes produced with CP and NS (d) mixes containing only MS and NS.

Further, in Figure 13b, it can be seen that the inclusion of 9% magnesium sulfate (CP0MS3 versus CP0MS9) slightly reduced the bands at  $\sim 1000\text{ cm}^{-1}$ . In Figure 13c, it can be seen that variations in mixes of 9% magnesium versus sodium sulfate did not change the FTIR bands considerably. These results agreed with those reported by Bakharev in [83], who exposed a coal fly ash (F)-based geopolymer to a sodium and magnesium sulfate solution and noted insignificant changes to the FTIR transmittance bands. Further, Figure 13d presents the effect of the magnesium and sodium sulfate content on mixes with 0% of ceramic powder. Based on this figure, the transmittance of mixes with 9% of magnesium sulfate appeared to experience lower bands compared to their companion mixes with 3% of magnesium sulfate. The lower intensity changes of specimens that were exposed to sodium sulfate versus those of magnesium sulfate were confirmed by Ref. [84].

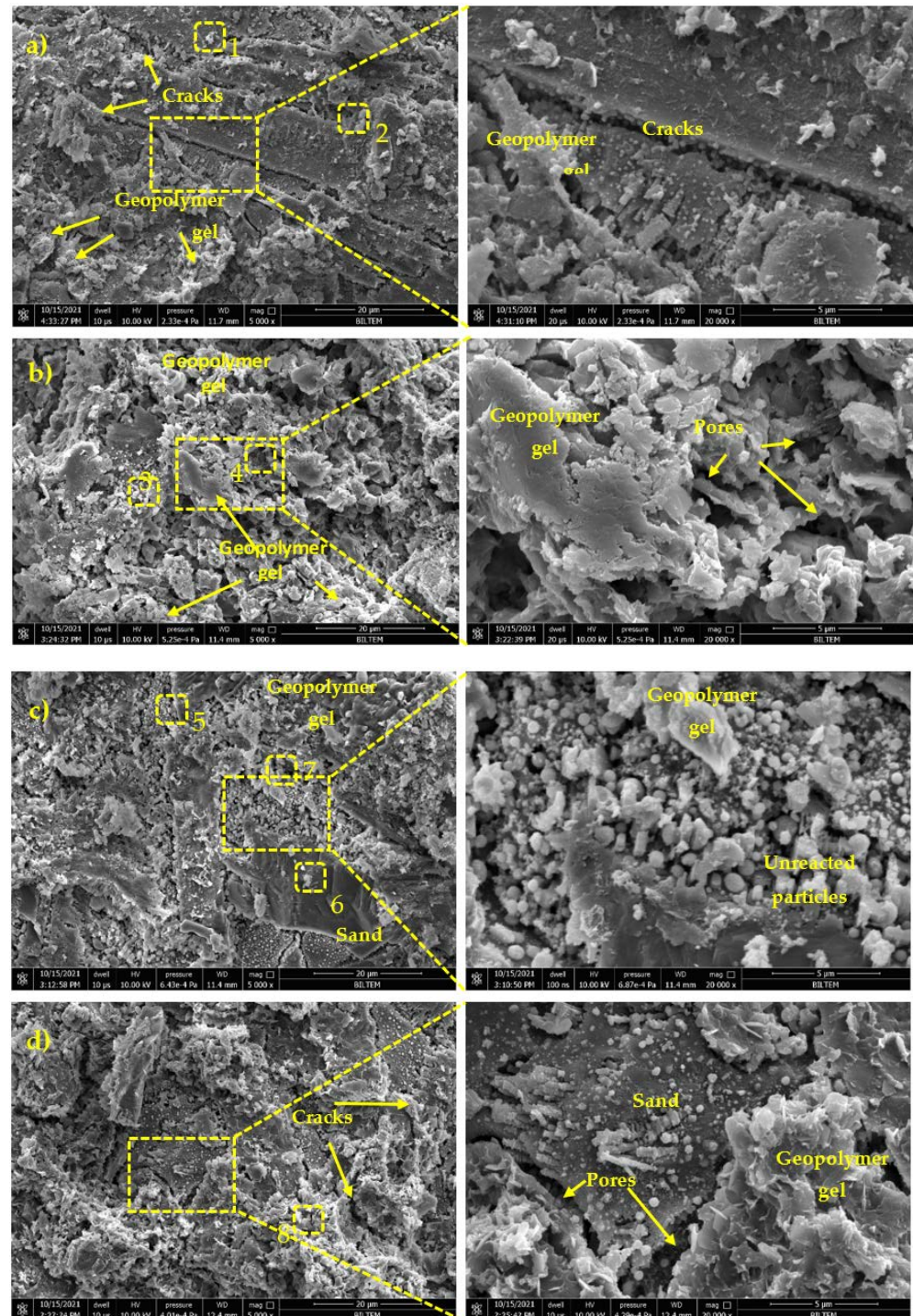
### 3.5.3. SEM and EDS

Figure 14a–d represent SEM micrographs with magnifications of  $20\ \mu\text{m}$  and  $5\ \mu\text{m}$  of fractured surfaces of specimens CP0, CP30, CP30NS9 and CP30MS9, following compression tests after 28 days of curing, respectively. The SEM micrograph of specimen CP0 demonstrated a highly heterogeneous microstructure with a significant portion of unreacted kaolin granules, revealing the lower dissolution of the kaolin precursor powder in this mix. On the other hand, a relatively more cohesive and denser geopolymer matrix could be seen in CP30 compared to CP0. This indicated that the increase in the concentration of ceramic powder from 0% to 30% caused a higher degree of dissolution of aluminosilicates and a powerful formation of geopolymer gels in CP30. By comparing Figure 14a,b, it can be seen that the sample incorporating 30% of ceramic powder had a lower porosity and a more consolidated microstructure than CP0. This illustrated the reason for the CP30 sample having a higher compressive strength than CP0. Additionally, the number of cracks and their respective widths were observed to be larger in CP0 as compared to CP30.

In the case of the geopolymer specimens incorporating 9%  $\text{Na}_2\text{SO}_4$  and 30% ceramic powder, as outlined in (Figure 14c), a consolidated microstructure was acquired with rare partially reacted particles. The images exhibited that the introduction of  $\text{Na}_2\text{SO}_4$  enhanced the uniformity degree of particles, allowing for their uniform dispersal within the matrix. Indeed, this reinforcement in the microstructure could be associated with an acceleration in the geopolymerization with the introduction of  $\text{Na}_2\text{SO}_4$  and the formation of more aluminosilicate gels. The results were in line with the findings of the study conducted by Qing-feng et al. [53], that the salt content might benefit the dissolution of aluminosilicate raw precursors and enhance the degree of geopolymerization [53]. On the other hand, it could be observed that CP30MS9 (Figure 14d) displayed a higher porosity and lower densification. This was because the lower pH of  $\text{MgSO}_4$  decreased the activation effect, leading to a high porosity and low compressive strength [67]. By comparing Figure 14c,d,



it could be seen that the geopolymer with  $\text{Na}_2\text{SO}_4$  had a more compact morphology than the mortar with  $\text{MgSO}_4$ . Moreover, the inclusion of 9% of sodium sulfate produced certain crystals that bridged the gaps in the microstructures of the produced geopolymers. This observation was consistent with the compressive strength test results (Figure 5), and could explain why CP0NS9 exhibited the maximum compressive strength recorded for all tested mortars.



**Figure 14.** SEM micrographs of mixes with magnification 20 and 5  $\mu\text{m}$ . (a) CP0; (b) CP30; (c) CP30NS9; (d) CP30MS9.

Table 4 represents the EDS analysis of the areas in Figure 14 marked from 1 to 8. The EDS table gives the dominant peaks for Al and Si and various minor peaks for Fe, Na, Mg, S, K and Ca due to precursors, the activator, aggregate and some supplements. To illustrate, in the first area of specimen CP0, the formation was thought to be a basalt aggregate due to the reasonable amount of Ca and Si peaks. However, the second area showed the presence of an acceptable amount of K, which was probably detected from the geopolymer gel. Additionally, the spectra of three and four also represented geopolymer gel formation, which was confirmed by the presence of Al, Si and K as the major elements. With the addition of  $\text{Na}_2\text{SO}_4$ , some minor peaks for Na were detected in the spectrum, namely, five and seven, in specimen CP30NS9. The presence of Ca and Si represented the basalt aggregate in spectrum six. The improvement in  $\text{Na}_2\text{SO}_4$  to the formation of geopolymer gel was also confirmed with the XRD analysis, which showed the reduced peaks for crystalline phases compared to the specimen without sodium sulfate. The EDS analysis indicated that spectrum eight represented the geopolymer gel, because of the higher contents of the elements Al, Si and K. It is noteworthy to mention that it was challenging to evaluate the geopolymerization rate for the specimens because of the small scan area.

**Table 4.** EDS (weight %) of CP0, CP30, CP30NS9 and CP30MS9.

Mix	EDS Area	O	Al	Si	Fe	Na	Mg	S	K	Ca
CP0	1	43.30	15.61	25.91	1.01	4.77	0.39	-	1.05	7.96
	2	47.65	9.63	25.92	2.85	3.25	1.03	-	5.76	3.91
CP30	3	46.13	8.53	23.36	3.93	2.55	2.29	-	10.97	2.24
	4	46.85	10.21	25.23	2.96	2.00	1.68	-	8.91	2.16
	5	40.30	7.28	30.27	7.29	2.82	1.03	2.96	5.52	3.17
CP30NS9	6	39.86	15.62	27.29	0.82	5.02	-	2.44	1.01	7.94
	7	42.37	10.60	24.40	3.37	6.59	0.95	2.60	4.66	4.45
CP30MS9	8	47.31	14.42	24.71	0.95	5.00	0.12	1.22	6.27	0.95

O: oxygen; Mg: magnesium; Al: aluminum; Si: silicon; S: sulfur; Ca: calcium.

#### 4. Conclusions

In this research study, the effect of sodium and magnesium sulfate on the mechanical and microstructural properties of kaolin and ceramic powder-based geopolymer concrete was evaluated. To that end, a total of 28 mixes was prepared with the kaolin content being replaced with ceramic powder at 0, 10, 20 and 30 vol.%. In the same way, sodium ( $\text{Na}_2\text{SO}_4$ ) and magnesium sulfate ( $\text{MgSO}_4$ ) were also added at 0, 3, 6 and 9 vol.% by substituting the kaolin content. Based on the results of this study, the following conclusions could be drawn:

- Replacing kaolin with ceramic powder increased the compressive and flexural strengths of the geopolymer mortars. This increase was attributed to the ceramic powder's higher specific surface area compared to kaolin, which created a denser matrix formation when replaced with kaolin. At a given ceramic powder content, the geopolymers containing  $\text{MgSO}_4$  exhibited lower strength values than those incorporating  $\text{Na}_2\text{SO}_4$ . This was due to the lower pH value of  $\text{MgSO}_4$  than  $\text{Na}_2\text{SO}_4$ , causing a porous matrix and leading to lower strengths.
- The porosity and water absorption of the geopolymers decreased when ceramic powder was replaced with kaolin. In addition, mortars containing  $\text{MgSO}_4$  exhibited higher porosity values than those with  $\text{Na}_2\text{SO}_4$ , showing sodium sulfate's contribution to geopolymerization, creating a denser microstructure. Additionally, a strong correlation is found to exist between the water absorption and porosity values in all mixes.
- UPV values were found to exhibit a very conforming trend with the unit weight, and showed a notable improvement with the increase in the ceramic powder content. Consistent with the compressive strength results, the increase in  $\text{Na}_2\text{SO}_4$  was found to increase the UPV values, as it contributed to the formation of gel and reduced the



void ratio. However,  $\text{MgSO}_4$  showed a decreasing trend in UPV values, indicating of a more porous structure.

- Through the XRD analyses, intense peaks for quartz, kaolinite, muscovite, anorthite and diopside were identified. A lowest quartz peak was observed in the geopolymer mortar incorporating 30% of ceramic powder with 9%  $\text{Na}_2\text{SO}_4$ , which showed that a combination of  $\text{Na}_2\text{SO}_4$  and ceramic powder could dissolve considerable parts of the crystalline phases and convert them into a semi-crystalline geopolymer gel, thereby contributing to the mechanical and microstructural properties of the geopolymers.
- The result of the FTIR in this study showed that the inclusion of ceramic powder slightly reduced the transmittance values, likely due to the penetration of  $\text{Al}^{4+}$  (tetrahedral aluminum atoms) into the reacting binder system. In the same way, the inclusion of sodium versus magnesium sulfate did not considerably alter the stretching vibrational bands, which could be due to the similar effect of the two compounds on the microstructural development of the geopolymer concrete.
- Based on the SEM images, the geopolymers without ceramic powder showed a heterogeneous microstructure with a considerable number of unreacted particles; however, a more coherent geopolymer matrix could be seen with the addition of the ceramic powder. Further to this, it is believed that sodium sulfate could bridge the crack gaps and accelerate the geopolymerization. This could lead to the formation of more aluminosilicate gel.

In the end, the results of this study were found to be significant and pointed to the suitability of utilizing ceramic powder and kaolin as precursors, activated, in part, using sodium and magnesium sulfate for the cleaner production of geopolymer concrete. Nonetheless, future studies in this area could provide further information on the thermo-durability properties of geopolymer concretes produced with sodium and magnesium sulfate.

**Author Contributions:** Conceptualization, M.K., F.K., O.G. and T.O.; methodology, M.K., F.K., O.G. and T.O.; software, M.K., F.K., O.G. and T.O.; validation, M.K., F.K., O.G. and T.O.; formal analysis, M.K., F.K., O.G. and T.O.; investigation, M.K., F.K., O.G. and T.O.; resources, M.K., F.K., O.G. and T.O.; data curation, M.K., F.K., O.G. and T.O.; writing—original draft preparation, M.N. and M.B.; writing—review and editing, M.N., M.B., O.G. and T.O.; visualization, M.N. and M.B.; supervision, M.K., F.K., O.G. and T.O.; project administration, M.K., F.K., O.G. and T.O.; funding acquisition, M.K., F.K., O.G. and T.O. All authors have read and agreed to the published version of the manuscript.

**Funding:** No funding was received for this study.

**Institutional Review Board Statement:** Not applicable.

**Informed Consent Statement:** Not applicable.

**Data Availability Statement:** Not applicable.

**Acknowledgments:** The authors acknowledge and appreciate all the institutions that supported this study.

**Conflicts of Interest:** The authors declare no conflict of interest.

## References

1. Nodehi, M.; Ozbakkaloglu, T.; Gholampour, A.; Mohammed, T.; Shi, X. The effect of curing regimes on physico-mechanical, microstructural and durability properties of alkali-activated materials: A review. *Constr. Build. Mater.* **2022**, *321*, 126335. [[CrossRef](#)]
2. McLellan, B.C.; Williams, R.P.; Lay, J.; Van Riessen, A.; Corder, G.D. Costs and carbon emissions for geopolymer pastes in comparison to ordinary portland cement. *J. Clean. Prod.* **2011**, *19*, 1080–1090. [[CrossRef](#)]
3. Heath, A.; Paine, K.; McManus, M. Minimising the global warming potential of clay based geopolymers. *J. Clean. Prod.* **2014**, *78*, 75–83. [[CrossRef](#)]
4. Passuello, A.; Rodríguez, E.D.; Hirt, E.; Longhi, M.; Bernal, S.A.; Provis, J.L.; Kirchheim, A.P. Evaluation of the potential improvement in the environmental footprint of geopolymers using waste-derived activators. *J. Clean. Prod.* **2017**, *166*, 680–689. [[CrossRef](#)]

5. Tang, Z.; Li, W.; Peng, Q.; Tam, V.W.; Wang, K. Study on the failure mechanism of geopolymeric recycled concrete using digital image correlation method. *J. Sustain. Cem. Mater.* **2022**, *11*, 113–126. [[CrossRef](#)]
6. Luo, Z.; Li, W.; Wang, K.; Shah, S.P.; Sheng, D. Nano/micromechanical characterisation and image analysis on the properties and heterogeneity of ITZs in geopolymer concrete. *Cem. Concr. Res.* **2022**, *152*, 106677. [[CrossRef](#)]
7. Qu, F.; Li, W.; Wang, K.; Zhang, S.; Sheng, D. Performance deterioration of fly ash/slag-based geopolymer composites subjected to coupled cyclic preloading and sulfuric acid attack. *J. Clean. Prod.* **2021**, *321*, 128942. [[CrossRef](#)]
8. Vinai, R.; Soutsos, M. Production of sodium silicate powder from waste glass cullet for alkali activation of alternative binders. *Cem. Concr. Res.* **2019**, *116*, 45–56. [[CrossRef](#)]
9. Adesanya, E.; Ohenoja, K.; Di Maria, A.; Kinnunen, P.; Illikainen, M. Alternative alkali-activator from steel-making waste for one-part alkali-activated slag. *J. Clean. Prod.* **2020**, *274*, 123020. [[CrossRef](#)]
10. Bianco, I.; Ap Dafydd Tomos, B.; Vinai, R. Analysis of the environmental impacts of alkali-activated concrete produced with waste glass-derived silicate activator—A LCA study. *J. Clean. Prod.* **2021**, *316*, 128383. [[CrossRef](#)]
11. Bajpai, R.; Choudhary, K.; Srivastava, A.; Sangwan, K.S.; Singh, M. Environmental impact assessment of fly ash and silica fume based geopolymer concrete. *J. Clean. Prod.* **2020**, *254*, 120147. [[CrossRef](#)]
12. Luukkonen, T.; Abdollahnejad, Z.; Yliniemi, J.; Kinnunen, P.; Illikainen, M. One-part alkali-activated materials: A review. *Cem. Concr. Res.* **2018**, *103*, 21–34. [[CrossRef](#)]
13. Danish, A.; Ozbakkaloglu, T.; Ali Mosaberpanah, M.; Salim, M.U.; Bayram, M.; Yeon, J.H.; Jafar, K. Sustainability benefits and commercialization challenges and strategies of geopolymer concrete: A review. *J. Build. Eng.* **2022**, *58*, 105005. [[CrossRef](#)]
14. Nodehi, M.; Taghvaei, V.M. Applying Circular Economy to Construction Industry through Use of Waste Materials: A Review of Supplementary Cementitious Materials, Plastics, and Ceramics. *Circ. Econ. Sustain.* **2022**, *2*, 987–1020. [[CrossRef](#)]
15. Okoye, F.N.; Durgaprasad, J.; Singh, N.B. Mechanical properties of alkali activated flyash/Kaolin based geopolymer concrete. *Constr. Build. Mater.* **2015**, *98*, 685–691. [[CrossRef](#)]
16. Firdous, R.; Stephan, D.; Djobo, J.N.Y. Natural pozzolan based geopolymers: A review on mechanical, microstructural and durability characteristics. *Constr. Build. Mater.* **2018**, *190*, 1251–1263. [[CrossRef](#)]
17. Figueiredo, R.A.M.; Brandão, P.R.G.; Soutsos, M.; Henriques, A.B.; Fourie, A.; Mazzinghy, D.B. Producing sodium silicate powder from iron ore tailings for use as an activator in one-part geopolymer binders. *Mater. Lett.* **2021**, *288*, 129333. [[CrossRef](#)]
18. Rajan, H.S.; Kathirvel, P. Sustainable development of geopolymer binder using sodium silicate synthesized from agricultural waste. *J. Clean. Prod.* **2021**, *286*, 124959. [[CrossRef](#)]
19. Adesanya, E.; Ohenoja, K.; Luukkonen, T.; Kinnunen, P.; Illikainen, M. One-part geopolymer cement from slag and pretreated paper sludge. *J. Clean. Prod.* **2018**, *185*, 168–175. [[CrossRef](#)]
20. Mohammed, T.; Aguayo, F.; Nodehi, M.; Ozbakkaloglu, T. Engineering properties of structural lightweight concrete containing expanded shale and clay with high volume class F and class C fly ash. *Struct. Concr.* **2022**. [[CrossRef](#)]
21. Nodehi, M.; Ozbakkaloglu, T.; Gholampour, A. Effect of supplementary cementitious materials on properties of 3D printed conventional and alkali-activated concrete: A review. *Autom. Constr.* **2022**, *138*, 104215. [[CrossRef](#)]
22. Moon, J.; Bae, S.; Celik, K.; Yoon, S.; Kim, K.H.; Kim, K.S.; Monteiro, P.J.M. Characterization of natural pozzolan-based geopolymeric binders. *Cem. Concr. Compos.* **2014**, *53*, 97–104. [[CrossRef](#)]
23. Tchadjie, L.N.; Ekolu, S.O. Enhancing the reactivity of aluminosilicate materials toward geopolymer synthesis. *J. Mater. Sci.* **2018**, *53*, 4709–4733. [[CrossRef](#)]
24. Ye, N.; Chen, Y.; Yang, J.; Liang, S.; Hu, Y.; Hu, J.; Zhu, S.; Fan, W.; Xiao, B. Transformations of Na, Al, Si and Fe species in red mud during synthesis of one-part geopolymers. *Cem. Concr. Res.* **2017**, *101*, 123–130. [[CrossRef](#)]
25. Pohl, W.L. *Economic Geology Principles and Practice: Metals, Minerals, Coal and Hydrocarbons*; John Wiley & Sons, Inc.: Hoboken, NJ, USA, 2011.
26. Bloodworth, A.; Highley, D.E.; Mitchell, C. British Geological Survey. *Struct. Surv.* **2002**, *20*, 21–33.
27. WHO. Bentonite, Kaolin, and Selected Clay Minerals. 2005. Available online: <https://apps.who.int/iris/handle/10665/43102> (accessed on 21 September 2022).
28. Zhang, Z.H.; Zhu, H.J.; Zhou, C.H.; Wang, H. Geopolymer from kaolin in China: An overview. *Appl. Clay Sci.* **2016**, *119*, 31–41. [[CrossRef](#)]
29. Daud, Y.M.; Hussin, K.; Osman, A.F.; Ghazali, C.M.R.; Al Bakri Abdullah, M.M.; Sandu, A.V. Dynamic mechanical properties of hybrid layered silicates/kaolin geopolymer filler in epoxy composites. *Mater. Plast* **2017**, *54*, 543–545. [[CrossRef](#)]
30. Sun, Z.; Cui, H.; An, H.; Tao, D.; Xu, Y.; Zhai, J.; Li, Q. Synthesis and thermal behavior of geopolymer-type material from waste ceramic. *Constr. Build. Mater.* **2013**, *49*, 281–287. [[CrossRef](#)]
31. Vincent, T.; Gholampour, A.; Ozbakkaloglu, T.; Ngo, T.D. Waste-based alkali-activated mortars containing low- and high-halloysite kaolin nanoparticles. *J. Clean. Prod.* **2021**, *327*, 129428. [[CrossRef](#)]
32. Khan, S.U.; Nuruddin, M.F.; Ayub, T.; Shafiq, N. Effects of different mineral admixtures on the properties of fresh concrete. *Sci. World J.* **2014**, *2014*, 986567. [[CrossRef](#)]
33. Penteado, C.S.G.; Viviani de Carvalho, E.; Lintz, R.C.C. Reusing ceramic tile polishing waste in paving block manufacturing. *J. Clean. Prod.* **2016**, *112*, 514–520. [[CrossRef](#)]
34. Huang, Y.; Luo, J.; Xia, B. Application of cleaner production as an important sustainable strategy in the ceramic tile plant—A case study in Guangzhou, China. *J. Clean. Prod.* **2013**, *43*, 113–121. [[CrossRef](#)]

35. Wang, Y.; Liu, Y.; Cui, S.; Sun, B.; Gong, X.; Gao, F.; Wang, Z. Comparative life cycle assessment of different fuel scenarios and milling technologies for ceramic tile production: A case study in China. *J. Clean. Prod.* **2020**, *273*, 122846. [CrossRef]
36. Kannan, D.M.; Aboubakr, S.H.; EL-Dieb, A.S.; Reda Taha, M.M. High performance concrete incorporating ceramic waste powder as large partial replacement of Portland cement. *Constr. Build. Mater.* **2017**, *144*, 35–41. [CrossRef]
37. Huseien, G.F.; Sam, A.R.M.; Mirza, J.; Tahir, M.M.; Asaad, M.A.; Ismail, M.; Shah, K.W. Waste ceramic powder incorporated alkali activated mortars exposed to elevated Temperatures: Performance evaluation. *Constr. Build. Mater.* **2018**, *187*, 307–317. [CrossRef]
38. Keppert, M.; Vejmelková, E.; Bezdička, P.; Doleželová, M.; Čáchová, M.; Scheinherrová, L.; Pokorný, J.; Vyšvařil, M.; Rovnaníková, P.; Černý, R. Red-clay ceramic powders as geopolymer precursors: Consideration of amorphous portion and CaO content. *Appl. Clay Sci.* **2018**, *161*, 82–89. [CrossRef]
39. Huseien, G.F.; Sam, A.R.M.; Shah, K.W.; Asaad, M.A.; Tahir, M.M.; Mirza, J. Properties of ceramic tile waste based alkali-activated mortars incorporating GBFS and fly ash. *Constr. Build. Mater.* **2019**, *214*, 355–368. [CrossRef]
40. Huseien, G.F.; Sam, A.R.M.; Shah, K.W.; Mirza, J.; Tahir, M.M. Evaluation of alkali-activated mortars containing high volume waste ceramic powder and fly ash replacing GBFS. *Constr. Build. Mater.* **2019**, *210*, 78–92. [CrossRef]
41. Kaya, M. The effect of micro-SiO<sub>2</sub> and micro-Al<sub>2</sub>O<sub>3</sub> additive on the strength properties of ceramic powder-based geopolymer pastes. *J. Mater. Cycles Waste Manag.* **2021**, *24*, 333–350. [CrossRef]
42. Baraldi, L. Ceramic World Review. 2015, pp. 48–63. Available online: [https://issuu.com/tiledizioni/docs/000\\_112\\_cwr\\_111/48](https://issuu.com/tiledizioni/docs/000_112_cwr_111/48) (accessed on 21 September 2022).
43. Heah, C.Y.; Kamarudin, H.; Mustafa Al Bakri, A.M.; Luqman, M.; Khairul Nizar, I.; Liew, Y.M. Potential application of kaolin without calcine as greener concrete: A review. *Aust. J. Basic Appl. Sci.* **2011**, *5*, 1026–1035.
44. Yankwa Djobo, J.N.; Elimbi, A.; Tchakouté, H.K.; Kumar, S. Mechanical activation of volcanic ash for geopolymer synthesis: Effect on reaction kinetics, gel characteristics, physical and mechanical properties. *RSC Adv.* **2016**, *6*, 39106–39117. [CrossRef]
45. Vafaei, M.; Allahverdi, A. Influence of calcium aluminate cement on geopolymerization of natural pozzolan. *Constr. Build. Mater.* **2016**, *114*, 290–296. [CrossRef]
46. Alnahhal, M.F.; Kim, T.; Hajimohammadi, A. Waste-derived activators for alkali-activated materials: A review. *Cem. Concr. Compos.* **2021**, *118*, 103980. [CrossRef]
47. Qin, L.; Gao, X.; Li, W.; Ye, H. Modification of Magnesium Oxysulfate Cement by Incorporating Weak Acids. *J. Mater. Civ. Eng.* **2018**, *30*, 04018209. [CrossRef]
48. Ma, C.; Zhao, B.; Wang, L.; Long, G.; Xie, Y. Clean and low-alkalinity one-part geopolymeric cement: Effects of sodium sulfate on microstructure and properties. *J. Clean. Prod.* **2020**, *252*, 119279. [CrossRef]
49. Cheah, C.B.; Tan, L.E.; Ramli, M. Recent advances in slag-based binder and chemical activators derived from industrial by-products—A review. *Constr. Build. Mater.* **2021**, *272*, 121657. [CrossRef]
50. NCBI. National Center for Biotechnology Information. PubChem Compound Summary for CID 24083, Magnesium Sulfate. 2021. Retrieved 1 November 2021. Available online: <https://pubchem.ncbi.nlm.nih.gov/compound/Magnesium-sulfate> (accessed on 5 March 2022).
51. Rashad, A.M.; Bai, Y.; Basheer, P.A.M.; Milestone, N.B.; Collier, N.C. Hydration and properties of sodium sulfate activated slag. *Cem. Concr. Compos.* **2013**, *37*, 20–29. [CrossRef]
52. Rattanasak, U.; Pankhet, K.; Chindaprasirt, P. Effect of chemical admixtures on properties of high-calcium fly ash geopolymer. *Int. J. Miner Metall. Mater.* **2011**, *18*, 364–369. [CrossRef]
53. Lv, Q.F.; Wang, Z.S.; Gu, L.Y.; Chen, Y.; Shan, X.K. Effect of sodium sulfate on strength and microstructure of alkali-activated fly ash based geopolymer. *J. Cent. South Univ.* **2020**, *27*, 1691–1702. [CrossRef]
54. Jun, Y.; Oh, J.-E. Microstructure and Strength of Class F Fly Ash based Geopolymer Containing Sodium Sulfate as an Additive. *J. Korea Concr. Inst.* **2015**, *27*, 443–450. [CrossRef]
55. Dal Pozzo, A.; Carabba, L.; Bignozzi, M.C.; Tugnoli, A. Life cycle assessment of a geopolymer mixture for fireproofing applications. *Int. J. Life Cycle Assess* **2019**, *24*, 1743–1757. [CrossRef]
56. Freilich, M.B.; Petersen, R.L. Potassium Compounds. In *Kirk-Othmer Encyclopedia of Chemical Technology*; John Wiley & Sons, Inc.: Hoboken, NJ, USA, 2014; pp. 1–35. [CrossRef]
57. Encyclopedia.com. Potassium Hydroxide | Encyclopedia.com. 2020. Available online: <https://www.encyclopedia.com/science/academic-and-educational-journals/potassium-hydroxide> (accessed on 21 April 2021).
58. Nodehi, M.; Taghvaei, V.M. Alkali-Activated Materials and Geopolymer: A Review of Common Precursors and Activators Addressing Circular Economy. *Circ. Econ. Sustain.* **2021**, *2*, 165–196. [CrossRef]
59. Reig, L.; Tashima, M.M.; Soriano, L.; Borrachero, M.V.; Monzó, J.; Payá, J. Alkaline activation of ceramic waste materials. *Waste Biomass Valorization* **2013**, *4*, 729–736. [CrossRef]
60. Mahmoodi, O.; Siad, H.; Lachemi, M.; Dadsetan, S.; Sahmaran, M. Development of ceramic tile waste geopolymer binders based on pre-targeted chemical ratios and ambient curing. *Constr. Build. Mater.* **2020**, *258*, 120297. [CrossRef]
61. Zhang, Z.; Wang, H.; Yao, X.; Zhu, Y. Effects of halloysite in kaolin on the formation and properties of geopolymers. *Cem. Concr. Compos.* **2012**, *34*, 709–715. [CrossRef]
62. Heah, C.Y.; Kamarudin, H.; Mustafa Al Bakri, A.M.; Bnhussain, M.; Luqman, M.; Khairul Nizar, I.; Ruzaidi, C.M.; Liew, Y.M. Kaolin-based geopolymers with various NaOH concentrations. *Int. J. Miner Metall. Mater.* **2013**, *20*, 313–322. [CrossRef]

63. Turkish Standards Institution A. Methods of Test for Mortar for Masonry—Part 11: Determination of Flexural and Compressive Strength of Hardened Mortar—CEN-EN 1015-11. Available online: <https://standards.globalspec.com/std/14245727/EN%201015-11> (accessed on 18 March 2022).
64. ASTM C642-13; Standard Test Method for Density, Absorption, and Voids in Hardened Concrete. Available online: <https://webstore.ansi.org/Standards/ASTM/astmc64213> (accessed on 18 March 2022).
65. Xu, H.; Van Deventer, J.S.J. The geopolymerisation of alumino-silicate minerals. *Int. J. Miner Process* **2000**, *59*, 247–266. [[CrossRef](#)]
66. Chithambar Ganesh, A.; Muthukannan, M. A review of recent developments in geopolymer concrete. *Int. J. Eng. Technol.* **2018**, *7*, 696–699. [[CrossRef](#)]
67. Activator, S.; Kang, C. Investigation of the Effects of Magnesium-Sulfate as Slag Activator. *Materials* **2020**, *13*, 305.
68. Li, Z.; Zhang, W.; Wang, R.; Chen, F.; Jia, X.; Cong, P. Effects of reactive MgO on the reaction process of geopolymer. *Materials* **2019**, *12*, 526. [[CrossRef](#)]
69. Rowles, M.; O'Connor, B. Chemical optimisation of the compressive strength of aluminosilicate geopolymers synthesised by sodium silicate activation of metakaolinite. *J. Mater. Chem.* **2003**, *13*, 1161–1165. [[CrossRef](#)]
70. Atiş, C.D.; Görür, E.B.; Karahan, O.; Bilim, C.; Ilkentapar, S.; Luga, E. Very high strength (120 MPa) class F fly ash geopolymer mortar activated at different NaOH amount, heat curing temperature and heat curing duration. *Constr. Build. Mater.* **2015**, *96*, 673–678. [[CrossRef](#)]
71. Song, S.; Sohn, D.; Jennings, H.M.; Mason, T.O. Hydration of alkali-activated ground granulated blast furnace slag. *J. Mater. Sci.* **2000**, *35*, 249–257. [[CrossRef](#)]
72. Puertas, F.; Fernández-Jiménez, A.; Blanco-Varela, M.T. Pore solution in alkali-activated slag cement pastes. Relation to the composition and structure of calcium silicate hydrate. *Cem. Concr. Res.* **2004**, *34*, 139–148. [[CrossRef](#)]
73. Galvão Souza Azevedo, A.; Strecker, K. Kaolin, fly-ash and ceramic waste based alkali-activated materials production by the “one-part” method. *Constr. Build. Mater.* **2021**, *269*, 121306. [[CrossRef](#)]
74. Şahin, F.; Uysal, M.; Canpolat, O.; Aygörmez, Y.; Cosgun, T.; Dehghanpour, H. Effect of basalt fiber on metakaolin-based geopolymer mortars containing rilem, basalt and recycled waste concrete aggregates. *Constr. Build. Mater.* **2021**, *301*, 124113. [[CrossRef](#)]
75. Cheah, C.B.; Samsudin, M.H.; Ramli, M.; Part, W.K.; Tan, L.E. The use of high calcium wood ash in the preparation of Ground Granulated Blast Furnace Slag and Pulverized Fly Ash geopolymers: A complete microstructural and mechanical characterization. *J. Clean. Prod.* **2017**, *156*, 114–123. [[CrossRef](#)]
76. Rovnaník, P.; Rovnaníková, P.; Vyšvařil, M.; Grzeszczyk, S.; Janowska-Renkas, E. Rheological properties and microstructure of binary waste red brick powder/metakaolin geopolymer. *Constr. Build. Mater.* **2018**, *188*, 924–933. [[CrossRef](#)]
77. Reig, L.; Soriano, L.; Borrachero, M.V.; Monzó, J.; Payá, J. Influence of calcium aluminate cement (CAC) on alkaline activation of red clay brick waste (RCBW). *Cem. Concr. Compos.* **2016**, *65*, 177–185. [[CrossRef](#)]
78. Xu, L.Y.; Alrefaei, Y.; Wang, Y.S.; Dai, J.G. Recent advances in molecular dynamics simulation of the N-A-S-H geopolymer system: Modeling, structural analysis, and dynamics. *Constr. Build. Mater.* **2021**, *276*, 122196. [[CrossRef](#)]
79. Chitsaz, S.; Tarighat, A. Estimation of the modulus of elasticity of N-A-S-H and slag-based geopolymer structures containing calcium and magnesium ions as impurities using molecular dynamics simulations. *Ceram. Int.* **2021**, *47*, 6424–6433. [[CrossRef](#)]
80. Yehualaw, M.D.; Hwang, C.L.; Vo, D.H.; Koyenga, A. Effect of alkali activator concentration on waste brick powder-based ecofriendly mortar cured at ambient temperature. *J. Mater. Cycles Waste Manag.* **2021**, *23*, 727–740. [[CrossRef](#)]
81. Chindapasirt, P.; De Silva, P.; Sagoe-Crentsil, K.; Hanjitsuwan, S. Effect of SiO<sub>2</sub> and Al<sub>2</sub>O<sub>3</sub> on the setting and hardening of high calcium fly ash-based geopolymer systems. *J. Mater. Sci.* **2012**, *47*, 4876–4883. [[CrossRef](#)]
82. Silva, I.; Castro-Gomes, J.P.; Albuquerque, A. Effect of immersion in water partially alkali-activated materials obtained of tungsten mine waste mud. *Constr. Build. Mater.* **2012**, *35*, 117–124. [[CrossRef](#)]
83. Bakharev, T. Durability of geopolymer materials in sodium and magnesium sulfate solutions. *Cem. Concr. Res.* **2005**, *35*, 1233–1246. [[CrossRef](#)]
84. Chen, S.; Zhang, Y.; Yan, D.; Jin, J.; Tian, Y.; Liu, Y.; Qian, X.; Peng, Y.; Fujitsu, S. The influence of Si/Al ratio on sulfate durability of metakaolin-based geopolymer. *Constr. Build. Mater.* **2020**, *265*, 120735. [[CrossRef](#)]